

## Burgers equation with correlated noise: Renormalization-group analysis and applications to directed polymers and interface growth

Ernesto Medina, Terence Hwa, and Mehran Kardar

*Physics Department, Massachusetts Institute of Technology, Cambridge, Massachusetts 02139*

Yi-Cheng Zhang

*Dipartimento di Fisica, Istituto Nazionale di Fisica Nucleare, piazzale de Aldo Moro 2, I-00185, Roma, Italy*

(Received 30 June 1988)

The Burgers equation is the simplest nonlinear generalization of the diffusion equation. We present a detailed dynamical renormalization-group analysis of this equation subject to random noise. The noise itself can be the product of another stochastic process and is hence allowed to have correlations in space and/or time. In dimensions higher than a critical  $d_c$  weak and strong noise lead to different scaling exponents, while for  $d < d_c$  any amount of noise is relevant resulting in strong-coupling behavior. In the absence of temporal correlations we find two regimes for  $d < d_c$ : either the hydrodynamic behavior is determined by white noise and correlations are unimportant, or correlations dominate and the resulting scaling exponents can be obtained *exactly*. With temporal correlations present, the hydrodynamic behavior is much more complex, as renormalization predicts a complicated dependence of the effective noise spectrum on frequency in certain regimes. The relevance of these results to two interesting problems is discussed. One is the anomalous transverse fluctuations of a directed polymer in a random medium, and the other is a description of a growing interface. Various recent numerical simulations are reviewed in the light of these results. For example, we show that an exponent identity observed in all simulations so far follows simply from the Galilean invariance of the equation in the absence of temporal correlations.

### I. INTRODUCTION AND SUMMARY

The dynamics and evolution of many degrees of freedom interacting through nonlinear equations leads to many complex patterns and collective behaviors. Renormalization-group techniques, successful in the study of static collective phenomena,<sup>1</sup> have been extended to dynamics and reveal a much more complicated structure of universality classes than the corresponding static case.<sup>2</sup> One of the simplest archetypes of nonlinear evolution is the Burgers equation for a vorticity-free, compressible fluid flow.<sup>3</sup> The deterministic equation can be solved exactly, and shows how "shock waves" arise naturally as a result of the nonlinearity.<sup>3</sup> Forster, Nelson, and Stephen (FNS) studied a stochastic version of the Burgers equation (along with several other models of fluid behavior) by dynamic renormalization-group (RG) techniques, and demonstrated that it exhibits nontrivial dynamic behavior below two dimensions.<sup>4</sup>

Recently there has been a renewed interest in the Burgers equation since it is found to arise naturally in a number of diverse contexts. Variants of this equation describe the growth of interfaces,<sup>5</sup> driven diffusion,<sup>6</sup> and the large time limit of the Sivashinski equation describing flame fronts.<sup>7</sup> One explanation for this wide range of applications is that the Burgers equation is the simplest generalization of the diffusion equation that contains relevant nonlinearities. With these recent applications in mind, here we undertake a more detailed description of the RG method. The FNS results<sup>4</sup> are extended to cases

where the stochastic noise has long-range correlations in space and time, and consequently discover a number of surprising results.

In the presence of a random force  $\mathbf{f}(\mathbf{x}, t)$ , the velocity field of the Burgers equation evolves as

$$\frac{\partial \mathbf{v}}{\partial t} + \lambda \mathbf{v} \cdot \nabla \mathbf{v} = \nu \nabla^2 \mathbf{v} + \mathbf{f}(\mathbf{x}, t), \quad (1.1)$$

where  $\nu$  is the viscosity and a coefficient  $\lambda$  has been introduced for convenience. This stochastic equation is related to a number of other useful models. Since  $\mathbf{v}$  is vorticity free, it can be written as  $\mathbf{v} = -\nabla h$ , with the scalar field  $h$  satisfying

$$\frac{\partial h}{\partial t} = \nu \nabla^2 h + \frac{\lambda}{2} (\nabla h)^2 + \eta(\mathbf{x}, t), \quad (1.2)$$

where  $\mathbf{f} = -\nabla \eta$ . (Note that the requirement  $\nabla \times \mathbf{v} = 0$  implies  $\nabla \times \mathbf{f} = 0$ .) This nonlinear differential equation describes fluctuations of a growing interface with  $\nu$  being the surface tension. The coefficient  $\lambda$  is proportional to the average growth velocity and arises because the surface slope is parallel transported in such growth processes. Equation (1.2) can be generalized to describe a profile in  $d$  spatial dimensions. A third variant of this equation is obtained by the nonlinear transformation  $W = \exp[(\lambda/2\nu)h]$ .  $W$  satisfies

$$\frac{\partial W}{\partial t} = \nu \nabla^2 W + \frac{\eta(\mathbf{x}, t)}{\lambda} W, \quad (1.3)$$

which is a diffusion equation with random sources and

sinks. It is in general related to directed polymers in random media,<sup>8</sup> and in the special case of two dimensions describes roughening of an interface by impurities.<sup>9</sup>

Two other related problems are worth mentioning. One is the fluctuations  $\phi$  in a driven diffusive system which satisfy<sup>6</sup>

$$\frac{\partial \phi}{\partial t} = D \nabla^2 \phi - \mathbf{w} \cdot \nabla \phi^2 - \nabla \cdot \mathbf{j}(\mathbf{x}, t). \quad (1.4)$$

The nonlinear term expresses the fact that the velocity at which a density fluctuation travels depends on its magnitude.<sup>6</sup> Although this is not identical to Burgers's equation, it is equivalent to it in one dimension. Finally, the Sivashinski equation<sup>7</sup> applied to the evolution of flame fronts takes the form

$$\frac{\partial h}{\partial t} = -v \nabla^2 h + \frac{\lambda}{2} (\nabla h)^2 - v' \nabla^4 h. \quad (1.5)$$

This is a deterministic equation with a band of linearly unstable modes at short wavelengths. It is believed that the chaotic behavior generated by these modes can be described by a stochastic noise acting on the long-wavelength modes, so that the long-time, large-distance behavior of this equation is identical to Eq. (1.2).<sup>7</sup>

It is usually assumed that the stochastic noise  $\eta(\mathbf{x}, t)$  has at most short-range correlations in space and time. However, if Eq. (1.1) is used to describe turbulence in the inertial range, so that the noise describes the effect of removing fast modes, this assumption may not be justified.<sup>10</sup> Here we consider cases where the noise term is allowed to have long-range correlations in space and/or time. In these cases the noise spectrum  $D(k, \omega)$  defined through

$$\langle \eta(\mathbf{k}, \omega) \eta(\mathbf{k}', \omega') \rangle = 2D(k, \omega) \delta^{d-1}(\mathbf{k} + \mathbf{k}') \delta(\omega + \omega') \quad (1.6)$$

has power-law singularities of the form  $D(k, \omega) \sim |\mathbf{k}|^{-2\rho} \omega^{-2\theta}$ . The renormalization-group procedure of FNS (Ref. 4) is now generalized to calculate various dynamic critical exponents and their dependence on  $\rho$  and  $\theta$ . Since there is no intrinsic length scale in the problem, various correlation functions obtain simple algebraic asymptotic limits. For example, height fluctuations in the interface equation (1.2) behave as

$$\langle |h(\mathbf{x}, t) - h(\mathbf{x}', t')|^2 \rangle \sim |\mathbf{x} - \mathbf{x}'|^{2\chi} f \left[ \frac{|t - t'|}{|\mathbf{x} - \mathbf{x}'|^z} \right], \quad (1.7)$$

where  $\chi$  is the "roughening exponent" for the interface, and the dynamic exponent  $z$  describes the scaling of relaxation times with length.<sup>2</sup>

Section II is devoted to calculation of the exponents  $\chi$  and  $z$ . Simple dimensional analysis indicates that in the absence of nonlinearities ( $\lambda=0$ ),  $z_0=2$  and  $\chi_0=(3-d)/2 + \rho + 2\theta$ . For  $d < d_c = 3 + 2\rho + 4\theta$  these results are not valid as  $\lambda$  becomes a relevant parameter and leads to new scaling which is probed by a one-loop renormalization procedure. The case  $\theta=0$  is studied first as it is a rather straightforward generalization of the FNS procedure,<sup>4</sup> and offers a good opportunity for a review of the mechanics of the RG scheme. The new results take on simple forms and can be understood intuitively. For spa-

tial correlations ( $\rho > 0$ ,  $\theta=0$ ), renormalization of the noise spectrum  $D(k)$  indicates two regimes. For small  $\rho$  the white noise generated under scaling is dominant and the exponents  $z_w(d)$  and  $\chi_w(d)$  associated with  $\rho=0$  are recovered. For  $\rho$  larger than  $\rho_c(d) = \chi_w + (d-1-z_w)/2$  the long-range part of  $D(k)$  takes over, leading to new correlated noise exponents. The exponents in this regime are obtained exactly from a simple Flory-type scaling<sup>11</sup> and equal  $z_F = (3+d-2\rho)/3$  and  $\chi_F = (3-d+2\rho)/3$ . These expressions for exponents are not valid for  $\rho > d/2$  as no stable interface exists for  $\chi > 1$ . The generalization to  $\theta \neq 0$  is studied next. Since all of the complexity that arises here comes from the temporal part alone, we have set  $\rho=0$  throughout most of this section for simplicity. (The results can be trivially extended to the general case of  $\rho \neq 0$ ,  $\theta \neq 0$  as pointed out in the text and in the appendices.) For this case, there is still the regime  $\theta < \theta_c(d)$  when the exponents  $z_w(d)$  and  $\chi_w(d)$  characteristic of short-range noise are observed. However, for  $\theta > \theta_c = \rho_c(d)/z_w(d)$  the exponents are not given by any simple rule. This is shown to result from the absence of Galilean invariance in the presence of temporally correlated noise. Also the fixed function  $D^*(\omega)$  becomes quite complicated for  $\theta_c < \theta < \frac{1}{2}$  as various intermediate frequency dependencies are generated. For  $\theta > \frac{1}{2}$ , the fixed function  $D^*(\omega)$  develops an essential singularity at  $\omega=0$  because increasingly more singular powers of  $\omega$  are generated under RG. No stable surface can exist in this regime for any finite  $d$  unless Eq. (1.2) is modified to include higher powers of  $(\nabla h)$ .

In Sec. III we take advantage of the mapping to Eq. (1.3) to describe the behavior of directed polymers in random media.<sup>8</sup> The noise  $\eta(\mathbf{x}, t)$  now describes the effect of impurities on the polymer. Typical transverse fluctuations  $|x|$  scale with the length  $t$  of the polymer as  $|x| \sim t^\nu$ . In all dimensions, for strong disorder  $\nu$  can be different from the random walk value of  $\frac{1}{2}$ , and is related to the dynamic exponent of the Burgers equation by  $\nu = 1/z$ . In two dimensions the polymer problem is equivalent to the interface of an Ising model.<sup>9</sup> Spatial correlations in  $\eta(\mathbf{x}, t)$  now describe the long-range effect of impurities on the interface.<sup>11</sup> As the exponent  $\rho$  varies from 0 to 1 the effect of impurities interpolates between random bonds and random fields. The exponent  $\nu$  also changes from  $\frac{2}{3}$  to 1 as a consequence. Preliminary descriptions of these results were presented earlier.<sup>11</sup> Since then an independent calculation on a similar model has been reported by Natterman.<sup>12</sup> Numerical studies of the hierarchical structure of optimal paths subject to such impurities are also presented.

Section IV discusses the growth problem described by Eq. (1.2). We start by explaining the origin of the dynamically generated nonlinearity, and its connection to lateral growth. We briefly review various numerical simulations of growth that have recently appeared. All numerical simulations agree with the predictions based on Eq. (1.2) for two dimensions (e.g.,  $z = \frac{3}{2}$ ). In the interesting case of  $d=3$ , although simulations rule out the trivial scaling  $z=2$ , the value of  $z$  is less certain with  $z \sim \frac{5}{3}$  being suggested.<sup>13</sup> Temporal correlations in  $\eta(\mathbf{x}, t)$ , i.e.,  $\theta \neq 0$ , can

originate from impurities that do not diffuse and impede the growth of the interface, they will invalidate the exponent identity  $\chi+z=2$ .

A variety of technically interesting results and computational tools are relegated to the appendixes. In Appendix A we prove a number of *exact* exponent identities (e.g., resulting from nonrenormalization of long-range correlated noise). The importance of Galilean invariance is emphasized in Appendix B. Because of this symmetry the vertex  $\lambda$  does not renormalize in the absence of temporal noise, and this leads to the exponent identity  $\chi+z=2$ . Numerical simulations in all dimensions are in agreement with this identity. The calculations leading to propagator renormalization are described in Appendix C, while similar computations for noise renormalization and vertex renormalization (with temporal noise) are explained in Appendixes D and E. Finally, a typical in-

tegral involved in the noise-noise contraction is worked out in detail in Appendix F.

## II. RENORMALIZATION WITH CORRELATED NOISE

### A. General procedure

It is more convenient to work with a scalar rather than a vector equation, and hence we shall focus on Eq. (1.2) describing an interface in  $d$  dimensions. After a Fourier transformation

$$h(\mathbf{x}, t) = \int_{-\infty}^{\infty} \int_{k < \Lambda} d\omega d^d k \frac{1}{(2\pi)^d} h(\mathbf{k}, \omega) e^{i(\mathbf{k}\cdot\mathbf{x} - \omega t)}, \quad (2.1)$$

this equation becomes

$$-i\omega h(\mathbf{k}, \omega) = -\nu k^2 h(\mathbf{k}, \omega) - \frac{\lambda}{2} \int \int d\Omega d^d q \frac{1}{(2\pi)^d} \mathbf{q}\cdot(\mathbf{k}-\mathbf{q}) h(\mathbf{q}, \Omega) h(\mathbf{k}-\mathbf{q}, \omega-\Omega) + \eta(\mathbf{k}, \omega). \quad (2.2)$$

Note that the momentum integrals are performed in the transverse  $d'=d-1$  dimensional space subject to an upper cutoff  $\Lambda$ .  $\Lambda$  plays the role of a "lattice spacing" in real space and will be scaled to 1. The noise  $\eta(\mathbf{x}, t)$  is assumed to have correlations in space and time. Such correlations arise if the noise is itself the result of removing "faster" degrees of freedom.<sup>10</sup> If  $\eta(\mathbf{x}, t)$  is related to uncorrelated (white) noise  $R(\mathbf{x}, t)$  through

$$\eta(\mathbf{x}, t) = \int_{-\infty}^t dt' \int_{-\infty}^{\infty} d^d \mathbf{x}' K(\mathbf{x}-\mathbf{x}', t-t') R(\mathbf{x}', t'), \quad (2.3)$$

then a long-range power-law decay of the kernel  $K$  results in algebraic correlations in  $\eta$ . For example, if asymptotically  $K(\mathbf{x}, t) \sim 1/(|\mathbf{x}|^{d'-\rho}|t|^{1-\theta})$ , then

$$\langle \eta(\mathbf{x}, t) \eta(\mathbf{x}', t') \rangle \sim |\mathbf{x}-\mathbf{x}'|^{2\rho-d'} |t-t'|^{2\theta-1}, \quad (2.4a)$$

and asymptotically as  $(\mathbf{k}, \omega) \rightarrow 0$ ,

$$\langle \eta(\mathbf{k}, \omega) \eta(\mathbf{k}', \omega') \rangle = 2D k^{-2\rho} \omega^{-2\theta} \delta^{d'}(\mathbf{k}+\mathbf{k}') \delta(\omega+\omega'). \quad (2.4b)$$

We are interested in correlations in the solution of Eq. (2.2) in the hydrodynamic limit  $(\mathbf{k}, \omega) \rightarrow 0$ . The average behavior of height fluctuations, for example, is described by Eq. (1.7), which after Fourier transformation reads

$$\langle h(\mathbf{k}, \omega) h(\mathbf{k}', \omega') \rangle = \delta^{d'}(\mathbf{k}+\mathbf{k}') \delta(\omega+\omega') |\mathbf{k}|^{z-d'-2\chi} \times f \left[ \frac{\omega}{|\mathbf{k}|^z} \right]. \quad (2.5)$$

The scaling information and hence the dynamic universality class of the Langevin equation is contained in the exponents  $\chi$  and  $z$ . [The exponent  $\chi$  is related to the con-

ventional hydrodynamic exponent  $\eta$  describing velocity power spectrum<sup>4</sup> through  $\chi = (2-d')/2 + (2-\eta-z)/2$ ]. These exponents are first studied by naive dimensional analysis: A change of scale  $\mathbf{x} \rightarrow b\mathbf{x}$  is accompanied by  $t \rightarrow b^z t$  and  $h \rightarrow b^\chi h$  (and the corresponding changes in Fourier space). After this rescaling, Eq. (1.2) transforms to

$$b^{\chi-z} \frac{\partial h}{\partial t} = \nu b^{\chi-2} \nabla^2 h + \frac{\lambda}{2} b^{2\chi-2} (\nabla h)^2 + b^{(\rho-d'/2)+(\theta-1/2)z} \eta, \quad (2.6)$$

where Eq. (2.4) is used to determine the scaling of noise  $\eta(\mathbf{x}, t)$ . Thus under this transformation the parameters change to

$$\begin{aligned} \nu &\rightarrow b^{z-2} \nu, \\ D &\rightarrow b^{2\rho-d'-2\chi+(2\theta+1)z} D, \\ \lambda &\rightarrow b^{\chi+z-2} \lambda. \end{aligned} \quad (2.7)$$

In the absence of the nonlinear term (i.e.,  $\lambda=0$ ), the equation is made scale invariant upon the choice of

$$\begin{aligned} z &= z_0 = 2, \\ \chi &= \chi_0 = \rho + 2\theta + (3-d)/2. \end{aligned} \quad (2.8)$$

A nonlinearity added to this scale invariant equation has a dimension  $y_\lambda^0 = z_0 + \chi_0 - 2 = \chi_0$ . For  $d > d_c = 3 + 2\rho + 4\theta$  a small nonlinearity scales to zero and is *irrelevant*, while for  $d < d_c$  the nonlinearity is *relevant* and grows under rescaling. Nontrivial exponents are expected for  $d < d_c$  in the presence of nonlinearities. This change of behavior at  $d_c$  is also reflected in a perturbation analysis to be described next.

Equation (2.2) can be rewritten as

$$h(\mathbf{k}, \omega) = G_0(\mathbf{k}, \omega) \eta(\mathbf{k}, \omega) - \frac{\lambda}{2} G_0(\mathbf{k}, \omega) \int \int d\Omega d^d q \frac{1}{(2\pi)^d} \mathbf{q} \cdot (\mathbf{k} - \mathbf{q}) h(\mathbf{q}, \Omega) h(\mathbf{k} - \mathbf{q}, \omega - \Omega), \quad (2.9)$$

with a bare propagator

$$G_0(\mathbf{k}, \omega) = \frac{1}{\nu k^2 - i\omega}. \quad (2.10)$$

Equation (2.9) is a convenient starting point for a perturbative calculation of  $h(\mathbf{k}, \omega)$  in powers of  $\lambda$  as indicated diagrammatically in Fig. 1. The graphic expansion is quite standard<sup>4</sup> with  $\rightarrow$  indicating the propagator  $G_0$  and  $\times$  depicting the noise  $\eta(\mathbf{k}, \omega)$ . The averaging over stochastic noise is performed using Eq. (2.4b), and the effective response function  $G(\mathbf{k}, \omega)$  [defined by  $h(\mathbf{k}, \omega) \equiv G(\mathbf{k}, \omega) \eta(\mathbf{k}, \omega)$ ] is given perturbatively in Fig. 2(a). The lowest-order (one-loop) correction is

$$G(\mathbf{k}, \omega) = G_0(\mathbf{k}, \omega) + 4 \left[ \frac{-\lambda}{2} \right]^2 G_0^2(\mathbf{k}, \omega) \times \int \int d\Omega d^d q \frac{1}{(2\pi)^d} \mathbf{q} \cdot (\mathbf{k} - \mathbf{q}) \mathbf{q} \cdot \mathbf{k} G_0(\mathbf{k} - \mathbf{q}, \omega - \Omega) G_0(\mathbf{q}, \Omega) G_0(-\mathbf{q}, -\Omega) 2D(\mathbf{q}, \Omega) + O(\lambda^4), \quad (2.11)$$

where the combinatorial factor of four represents possible noise contractions leading to Fig. 2(a). Calculating the integrals is reasonably complicated and not particularly instructive (they are performed in Appendix C). For spatial correlations [ $D(\mathbf{q}, \Omega) = Dq^{-2\rho}$ ], after performing the frequency integrals and letting  $\omega \rightarrow 0$  we obtain Eqs. (C2) and (C3) (Appendix C) leading to

$$G(\mathbf{k}, 0) = G_0(\mathbf{k}, 0) + \left[ \frac{\lambda^2 D}{\nu^2} \right] G_0^2(\mathbf{k}, \omega) \left[ \frac{d' - 2 - 2\rho}{4d'} \right] k^2 \times \int d^d q \frac{1}{(2\pi)^{d'}} q^{-2(1+\rho)}, \quad (2.12)$$

where terms of the order of  $k^2$  are kept. Since  $G_0(k, 0) = 1/(\nu k^2)$ , this allows us to determine an effective surface tension  $\tilde{\nu}$  from  $G(k, 0) = 1/(\tilde{\nu} k^2)$ . From Eq. (2.12) the first-order correction of surface tension from nonlinearity takes the form

$$\tilde{\nu} = \nu \left[ 1 - \frac{\lambda^2 D}{\nu^3} \frac{d' - 2 - 2\rho}{4d'} \int d^d q \frac{1}{(2\pi)^{d'}} q^{-2(1+\rho)} \right]. \quad (2.13)$$

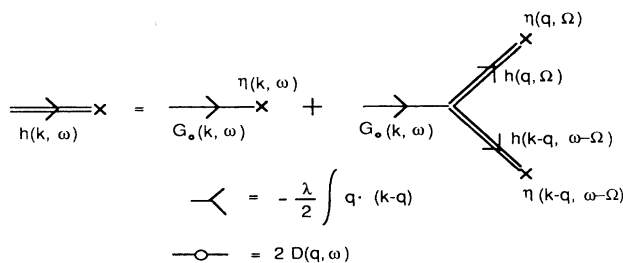


FIG. 1. Diagrammatic representation of the nonlinear integral equation (2.9), and the perturbation series that results from it.

The correction term is well behaved and finite for  $d' > 2(1 + \rho)$ , but diverges for  $d' < 2(1 + \rho)$ . This is another indication of relevance of nonlinearities and occurrence of nontrivial scaling behavior.

An effective spectral function  $\tilde{D}(k, \omega)$  can be defined from

$$\langle h^*(\mathbf{k}, \omega) h(\mathbf{k}, \omega) \rangle = 2G(\mathbf{k}, \omega) G(-\mathbf{k}, -\omega) \tilde{D}(\mathbf{k}, \omega).$$

This quantity is calculated perturbatively by the series shown in Fig. 2(b). The first correction term gives

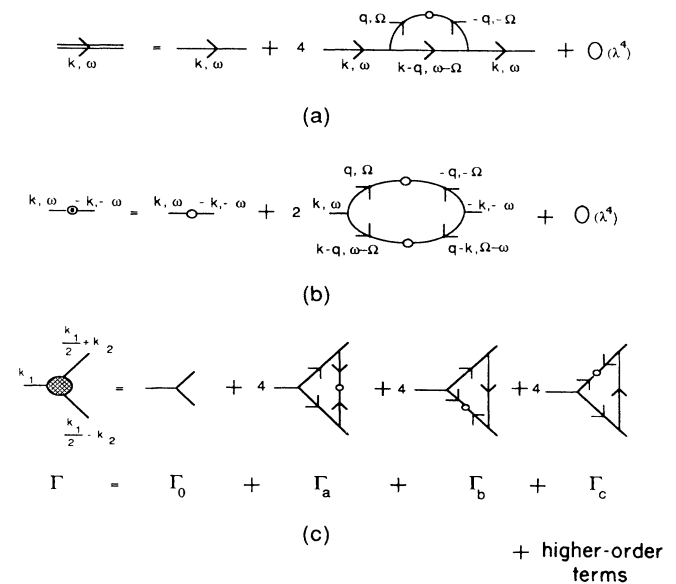


FIG. 2. After averaging over the noise, the perturbation series of Fig. 1 can be reorganized to describe (a) an effective propagator or response function, (b) an effective noise spectral density function, and (c) an effective vertex function or coupling constant.

$$\begin{aligned}
2\tilde{D}(\mathbf{k}, \omega) = & 2D(\mathbf{k}, \omega) + 2 \left[ \frac{-\lambda}{2} \right]^2 \int \int d\Omega d^{d'} q \frac{1}{(2\pi)^{d'}} [\mathbf{q} \cdot (\mathbf{k} - \mathbf{q})]^2 \\
& \times G_0(\mathbf{q}, \Omega) G_0(-\mathbf{q}, -\Omega) G_0(\mathbf{k} - \mathbf{q}, \omega - \Omega) G_0(-\mathbf{k} + \mathbf{q}, -\omega + \Omega) \\
& \times 2D(\mathbf{q}, \Omega) 2D(\mathbf{k} - \mathbf{q}, \omega - \Omega) + O(\lambda^4). \tag{2.14}
\end{aligned}$$

This expression is evaluated in Appendix D and again the perturbative correction is found to diverge for  $d < d_c$ . Similarly an effective "nonlinearity"  $\tilde{\lambda}$  is defined graphically in Fig. 2(c). This quantity, as calculated in Appendix E, is also divergent for  $d < d_c$ .

The divergences in perturbation series arise from the  $q \rightarrow 0$  limit of the integrals depicted in Figs. 2. The renormalization-group procedure amounts to a resummation of the perturbation series to avoid this singularity. The various steps of the program are outlined here.

(1) The averaging (i.e., the integrations in Figs. 2) is performed only over fluctuations with momenta  $k$  in the range  $\Lambda e^{-l} \leq k \leq \Lambda$ . As there are no singularities in this range of integration, only analytic corrections to  $\tilde{v}$ ,  $\tilde{D}$ , and  $\tilde{\lambda}$  result after elimination of the fast modes.

(2) After step (1) the resulting equation has a cutoff of  $\Lambda e^{-l}$ . This difference from the original model is removed by rescaling momenta  $k \rightarrow k e^{-l}$  which is identical to the scaling carried out earlier with  $b = e^l$ . The parameters  $\nu$ ,  $D$ , and  $\lambda$  are rescaled as in Eq. (2.7) with additional corrections arising from the integrations in step (1).

(3) As in Eq. (2.8), the exponents  $\chi$  and  $z$  are obtained by requiring that the parameters stay fixed; i.e., by making the equation invariant under the rescaling transformation. (Note that the freedom to choose  $\lambda$  makes it possible to leave all three parameters fixed).

The scaling of fluctuations also follows from the renormalization transformations. For example, scale invariance implies

$$\begin{aligned}
\langle |h(\mathbf{x}, t) - h(0, 0)|^2 \rangle \\
= e^{2\chi l} \langle |h(e^{-l}\mathbf{x}, e^{-z}t) - h(0, 0)|^2 \rangle, \tag{2.15}
\end{aligned}$$

and the choice of  $e^l \sim |\mathbf{x}|$  leads to the form

$$\langle |h(\mathbf{x}, t) - h(0, 0)|^2 \rangle \sim |\mathbf{x}|^{2\chi} f(t/x^z),$$

as indicated in Eq. (1.7). The actual implementation of steps (1)–(3) is demonstrated by specific examples in Secs. II B and II C and the detailed calculations leading to the renormalization recursion relations are given in the appendixes.

## B. Spatial correlations

First we consider the case where the noise has only spatial correlations but with a general form  $D(k)$  rather than the special case in Eq. (2.4b). Although, as we shall see later on, only the  $k \rightarrow 0$  limit of  $D(k)$  is responsible for the scaling behavior, here the three steps outlined previously will be carried out to give a quite general functional recursion relation for  $D(k)$ .

(1) The first step is to divide the Brillouin zone  $k \in [0, \Lambda]$  in two parts: high momenta  $k > \in [\Lambda e^{-l}, \Lambda]$  to be integrated out, and the remaining long wavelengths  $k < \in [0, \Lambda e^{-l}]$ . The integration of fast modes results in an effective propagator  $G^<(k, \omega)$  for the remaining modes. The  $\omega \rightarrow 0$  limit of this propagator calculated from Eq. (2.11) after manipulations similar to those in Appendix C is

$$G^<(k, 0) = G_0(k, 0) + G_0^2(k, 0) \frac{\lambda^2}{2\nu^2} \int^> d^{d'} q \frac{1}{(2\pi)^{d'}} \frac{\left[ q^2 - \frac{k^2}{4} \right] \left[ \mathbf{q} \cdot \mathbf{k} + \frac{k^2}{2} \right]}{\left[ \mathbf{q} + \frac{\mathbf{k}}{2} \right]^2 \left[ q^2 + \frac{k^2}{4} \right]} D \left[ q + \frac{k}{2} \right]. \tag{2.16}$$

The form of the new propagator is more complicated than the initial  $1/(\nu k^2)$ , as it contains  $k^4$  and  $k^6$  terms and so on. However, as the hydrodynamic behavior is completely determined by the small- $k$  limit, the expression in Eq. (2.16) is expanded in powers of  $k$ . As in Eq. (2.13) we can define an effective surface tension  $\nu^<$  for the long-wavelength modes by

$$\nu^< = \nu \left\{ 1 - \frac{\lambda^2}{2\nu^3} \int^> d^{d'} q \frac{1}{(2\pi)^{d'}} \frac{D(q)}{q^2} \left[ \frac{1}{2} - \frac{(\mathbf{q} \cdot \mathbf{k})^2}{q^2 k^2} \left[ 1 - \frac{f(q)}{2} \right] \right] \right\}. \tag{2.17}$$

The integration  $\int^> d^{d'} q$  is over a shell  $[\Lambda e^{-l}, \Lambda]$ , and  $f(q) = \partial \ln D(q) / \partial \ln q$ . Using spherical coordinates and an infinitesimal  $l$ , the integral is easily evaluated to

$$\nu^< = \nu \left[ 1 - \frac{\lambda^2 D(1)}{\nu^3} K_{d'} l \left[ \frac{d' - 2 + f(1)}{4d'} \right] \right], \tag{2.18}$$

where  $K_{d'} = S_{d'} / (2\pi)^{d'}$  and  $S_{d'}$  is the surface area of a unit sphere in  $d'$  dimensions. Without loss of generality the cutoff  $\Lambda$  is set to unity.

The effective noise acting on the long-wavelength modes can be calculated similarly starting from Eq. (2.14). After performing the frequency integrals

$$D^<(k) = D(k) + \frac{\lambda^2}{2\nu^3} \int^> d^{d'} q \frac{1}{(2\pi)^{d'}} \frac{[\mathbf{q} \cdot (\mathbf{k} - \mathbf{q})]^2 D(q) D(k - q)}{q^2 (\mathbf{k} - \mathbf{q})^2 [q^2 + (\mathbf{k} - \mathbf{q})^2]}. \quad (2.19)$$

In the same spirit as before we concentrate on the correction term only as  $k \rightarrow 0$ , and find after performing the shell integration

$$D^<(k) = D(k) + \frac{\lambda^2}{4\nu^3} K_{d'} D^2(1) l. \quad (2.20)$$

Thus any type of noise under renormalization generates a white-noise (i.e.,  $k$ -independent) contribution. The third parameter to consider is the coefficient  $\lambda$  of the non-linearity which has contributions coming from the graphs in Fig. 2(c). The integrations as described in Appendix E give a null result for spatial correlations. This is due to a Galilean invariance that is preserved under renormalization, and thus  $\lambda^< = \lambda$ . Galilean invariance is discussed in detail in Appendix B.

(2) Thus after short wavelengths are integrated out, the remaining modes are subject to the parameters calculated in (1). The only difference with the original Eq. (2.2) is that the allowed  $k$  are in the range 0 to  $e^{-l}$ . This difference is eliminated by reparametrizations  $k \rightarrow e^{-l} k$ ,  $h \rightarrow e^{\chi l} h$ , and  $t \rightarrow e^{z l} t$ . The result is similar to Eq. (2.7) with  $b = e^l$ . Combining these contributions for infinitesimal  $l$  with those calculated in Eqs. (2.18) and (2.20) leads to the differential recursion relations:

$$\frac{d\nu}{dl} = \nu \left[ z - 2 - K_{d'} \frac{\lambda^2 D(1)}{\nu^3} \left[ \frac{d-2+f(1)}{4d'} \right] \right], \quad (2.21a)$$

$$\frac{dD(k)}{dl} = D(k) [z - 2\chi - d' - f(k)] + K_{d'} \frac{\lambda^2}{4\nu^3} D^2(1), \quad (2.21b)$$

$$\frac{d\lambda}{dl} = \lambda [\chi + z - 2]. \quad (2.21c)$$

(3) The next step is to choose  $z$  and  $\chi$  such that the parameters are unchanged. Setting  $d\nu/dl = 0$  and  $d\lambda/dl = 0$ , Eqs. (2.21a) and (2.21c) become

$$\begin{aligned} z &= 2 + K_{d'} \frac{\lambda^2 D(1)}{\nu^3} \left[ \frac{d'-2+f(1)}{4d'} \right], \\ \chi &= -K_{d'} \frac{\lambda^2 D(1)}{\nu^3} \left[ \frac{d'-2+f(1)}{4d'} \right]. \end{aligned} \quad (2.22)$$

Substituting these into (2.21b) yields

$$\begin{aligned} \frac{dD(k)}{dl} &= [2 - d' - f(k)] D(k) \\ &+ 3K_{d'} \left[ \frac{d'-2+f(1)}{4d'} \right] \frac{\lambda^2 D(k) D(1)}{\nu^3} \\ &+ \frac{K_{d'} \lambda^2 D^2(1)}{4\nu^3}, \end{aligned}$$

and starting from any  $D(k)$  its renormalization can be followed from this equation. For any function that is finite at  $k=0$  the fixed function will be a constant [ $D^*(k) = D_0^*$ , i.e., white noise]. If initially  $D(k) \sim k^{-2\rho}$  as  $k \rightarrow 0$ , this singularity is preserved under renormalization, while a white-noise component is also generated.

The noise spectrum now approaches a form  $D(k) = D_0 + D_\rho k^{-2\rho}$ . In terms of the dimensionless parameters  $U_0 \equiv K_{d'} \lambda^2 D_0 / \nu^3$ ,  $U_\rho \equiv K_{d'} \lambda^2 D_\rho / \nu^3$  we have

$$\begin{aligned} \frac{dU_0}{dl} &= U_0(2 - d') + U_0^2 \left[ \frac{3}{4} \frac{d'-2}{d'} + \frac{1}{4} \right] + \frac{U_\rho^2}{4} \\ &+ U_0 U_\rho \left[ \frac{5d'-6\rho-6}{4d'} \right], \end{aligned} \quad (2.23a)$$

$$\begin{aligned} \frac{dU_\rho}{dl} &= U_\rho(2 - d' + 2\rho) + U_\rho^2 \left[ \frac{3}{4d'} (d' - 2 - 2\rho) \right] \\ &+ U_0 U_\rho \left[ \frac{3(d'-2)}{4d'} \right]. \end{aligned} \quad (2.23b)$$

From these recursion relations we can solve for fixed points (points at which parameters are unchanged under rescaling) and determine the flows in  $(U_0, U_\rho)$  space as a function of  $\rho$  and the dimensionality of space  $d$ . The results are shown in Fig. 3, where a variety of qualitative behaviors are apparent.

In region A we observe that for small  $\rho$  the long-range part of the correlations is irrelevant, i.e.,  $U_\rho^* = 0$ ; so we have a fixed point on the  $U_0$  axis and the exponents

$$z_w = 2 + \frac{(d'-2)^2}{4d'-6}, \quad (2.24)$$

$$\chi_w = \frac{(d'-2)^2}{6-4d'},$$

associated with  $\rho=0$  are obtained. These exponents are arrived at by substituting the fixed values of  $U_0^*$  and  $U_\rho^*$  into the equations for  $z$  and  $\chi$ . For larger values of  $\rho$ , namely, for

$$\rho > \rho_c(d') = \chi_w(d') + \frac{d' - z_w(d')}{2} = \frac{d'(d'-2)}{8(d'-\frac{3}{2})}, \quad (2.25)$$

(region B in the diagram), the long-range part of  $D(k)$  takes over, leading to new exponents. As shown in Fig. 3, an off-axis fixed point is obtained and the exponents are given by

$$\begin{aligned} z(\rho) &= 1 + \frac{d'+1-2\rho}{3}, \\ \chi(\rho) &= 1 + \frac{2\rho-d'-1}{3}. \end{aligned} \quad (2.26)$$

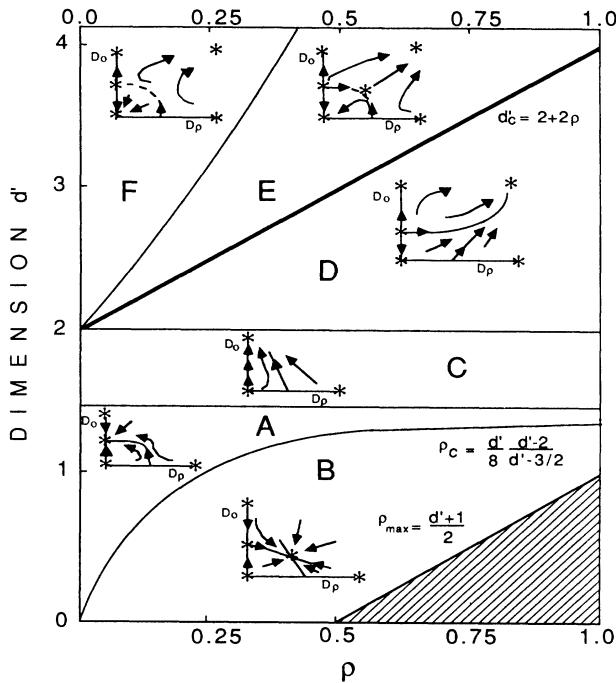


FIG. 3. Distinct behaviors of renormalization group flows in  $(d', \rho)$  space for  $\theta=0$  (no temporal correlations) calculated to one-loop order. The solid line  $d'_c = 2 + 2\rho$  represents the upper critical dimension. For  $d > d'_c$  both weak-coupling and strong-coupling regimes exist. The fixed point moves off axis in going from A to B, and in the shaded regime the exponent  $\chi$  is larger than unity so our procedure is not applicable.

These exponents are depicted in Fig. 4 for  $d=2$ . It is worth emphasizing that in the case of  $d'=1$  ( $d=2$ ) the results obtained from these one-loop calculations are actually exact. This is a consequence of certain exponent identities, as discussed in Appendix A.

From Eq. (2.26) we see that noise with very-long-range correlation (i.e., large  $\rho$ ) tends to roughen the surface (increase roughening exponent  $\chi$ ) while a high dimensionality tends to stabilize or smoothen the surface. For  $\chi \geq 1$ ,  $\nabla h \rightarrow b^{\chi-1}h$  starts to grow under rescaling and higher-order nonlinearities become relevant. Hence the range of  $\rho$  for which Eq. (1.2) describes a well-behaved surface is by Eq. (2.26)

$$\rho < \rho_{\max} = \frac{d'+1}{2}.$$

Beyond this limit, Eq. (1.2) must be modified to include higher powers of  $\nabla h$ .

Interesting behavior is also observed above the line which defines the critical dimensionality (where small nonlinearities are irrelevant). This regime [regions E and F in Fig. (3)] allows for a phase transition between an "ideal" phase (weak-coupling limit  $U_0 = U_\rho = 0$ ) characterized by the exponent  $z=2$ , and a strong-coupling limit (where flows go to infinity) not accessible by this perturbative scheme. The phase boundary is depicted by a dashed line in Fig. 3, and is controlled by an unstable fixed point. This fixed point emerges from the origin and follows a trajectory that ends as it merges into the  $U_0$

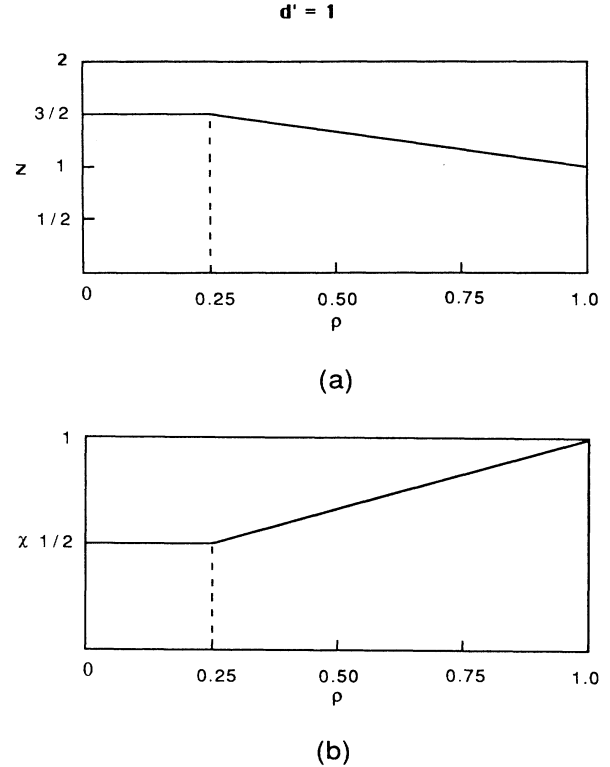


FIG. 4. (a) Dynamic exponent  $z$  and (b) roughening exponent  $\chi$  as a function of the exponent  $\rho$  for decay of spatial correlations, in  $d=2$  ( $d'=1$ ).

axis when crossing into region F. The exponents for this critical fixed point are also given by Eqs. (2.24) and (2.25).

Finally, in the two regions C and D observed in the diagram, no stable fixed points are found for finite  $U_0$  and  $U_\rho$ . On the  $d'=2$  line itself the coupling is marginally relevant, and hence a flow similar to region D is attained. In these regions, the perturbative calculation must be carried out to higher order (two- and three-loop diagrams) in order to evaluate the exponents. It is clearly observed in all regimes (see Fig. 3) that white noise is always generated under renormalization. The flows that begin near the  $U_\rho$  axis (only  $k^{-2\rho}$  correlations) generate a  $U_0 \neq 0$  component as was pointed out before. In the derivation of the exponents  $z$  and  $\chi$  above, we have been using the expression

$$\chi + z = 2 \quad (2.27)$$

(which was derived from setting  $d\lambda/dl=0$ ). In fact this is an identity as a consequence of the Galilean invariance of Eq. (1.2) (see Appendix B) in the presence of whatever correlations that preserve this symmetry, and is valid to all orders of perturbation theory. We shall see in Section IIC that in the presence of temporal correlations this symmetry is broken and the identity no longer holds.

As is clear from our description, this perturbative analysis is distinguished from a traditional  $\epsilon$  expansion, where one expands around the critical dimension of the system (above which the critical behavior is of the weak-

coupling mean-field type) to obtain access to lower dimensions where the exponents are nontrivial.<sup>1</sup> The one-loop calculation is uncontrolled since the fixed point value of the coupling constant cannot be controlled in a perturbative fashion about  $\epsilon = d'_c - d'$ . As seen in Fig. 3 there is no fixed point from Eqs. (2.23) for small  $\epsilon$ , and fixed points first appear in region A.

### C. Temporal correlations

The renormalization procedure used in Sec. II B is now generalized to arbitrary spectral functions  $D(k, \omega)$ . After going through the calculations outlined in Appendixes C, D, and E, we arrive at the following set of differential recursion relations for the functional renormalization of  $D(k, \omega)$ :

$$\frac{d\nu}{dl} = \nu \left[ z - 2 - K_{d'} \frac{\lambda^2 \tilde{D}_1(1)}{\nu^3} \left( \frac{d' - 2 + \tilde{f}(1)}{4d'} \right) \right], \quad (2.28a)$$

$$\begin{aligned} \frac{dD(k, \omega)}{dl} = D(k, \omega) \left[ z \left( 1 - \frac{\partial \ln D}{\partial \ln \omega} \right) - 2\chi - d' - \frac{\partial \ln D}{\partial \ln k} \right] \\ + K_{d'} \frac{\lambda^2}{4\nu^3} \tilde{D}_2^2(\omega), \end{aligned} \quad (2.28b)$$

$$\frac{d\lambda}{dl} = \lambda \left[ \chi + z - 2 - K_{d'} \frac{\lambda^2 \tilde{D}_3}{\nu^3} \frac{1}{2d'} \right], \quad (2.28c)$$

where  $\tilde{f}$  and  $\tilde{D}$ 's involve various integrals of  $D(k, \omega)$ , their exact forms are given by Eqs. (C1), (D1), and (E1). Equations (2.28) yield a nonlinear integral-differential equation for the fixed function  $D^*(k, \omega)$  when the exponents are chosen such that  $d\nu/dl = 0 = d\lambda/dl$ . Solving such an equation is difficult and is not very instructive.

Motivated by the form of the fixed function  $D^*(k, \omega)$  of Sec. II B, we look for a fixed function of the form  $D(k, \omega) = D_0 + D_\theta k^{-2\rho(\omega/\omega_0)^{-2\theta}}$ , where the factor  $\omega_0 = \nu \Lambda^2$  ( $=\nu$  for  $\Lambda=1$ ) is included to make the argument dimensionless. [The more complicated case involving nonseparable  $D(k, \omega)$  will not be treated here.] The relevant integrals needed to obtain  $\tilde{D}$ 's are evaluated using contour integration (an example will be shown later in Appendix F). The results are

$$\tilde{D}_1(1) = D_0 + D_\theta (1 + 2\theta) \sec(\pi\theta), \quad 0 \leq \theta \leq \frac{1}{2}$$

$$\tilde{D}_1(1) \tilde{f}(1) = -2\rho D_\theta (1 + 2\theta) \sec(\pi\theta), \quad 0 \leq \theta < \frac{1}{2}$$

$$\begin{aligned} \tilde{D}_2^2(\omega) &= D_0^2 + 2D_0 D_\theta (1 + 2\theta) \sec(\pi\theta) \\ &+ D_\theta^2 (1 + 4\theta) \sec(2\pi\theta), \quad 0 \leq \theta < \frac{1}{4} \end{aligned}$$

$$\tilde{D}_3 = -D_\theta 2\theta (1 + 2\theta) \sec(\pi\theta), \quad 0 \leq \theta < \frac{1}{2}.$$

Expressed in terms of dimensionless parameters  $U_0 = K_{d'} \lambda^2 D_0 / \nu^3$  and  $U_\theta = K_{d'} \lambda^2 D_\theta / \nu^3$ , the recursion relations are

$$\begin{aligned} \frac{d\nu}{dl} = \nu \left[ z - 2 + U_0 \frac{2 - d'}{4d'} \right. \\ \left. + U_\theta \frac{2 - d' + 2\rho}{4d'} (1 + 2\theta) \sec(\pi\theta) \right], \end{aligned} \quad (2.29a)$$

$$\frac{d\lambda}{dl} = \lambda \left[ \chi + z - 2 + U_\theta \frac{\theta}{d'} (1 + 2\theta) \sec(\pi\theta) \right], \quad (2.29b)$$

$$\frac{dU_\theta}{dl} = U_\theta [z(1 + 2\theta) - 2\chi - d' + 2\rho], \quad (2.29c)$$

$$\begin{aligned} \frac{dU_0}{dl} = U_0 (z - 2\chi - d') + \frac{1}{4} U_0^2 + \frac{1}{2} U_0 U_\theta (1 + 2\theta) \sec(\pi\theta) \\ + \frac{1}{4} U_\theta^2 (1 + 4\theta) \sec(2\pi\theta), \end{aligned} \quad (2.29d)$$

valid for  $\theta < \frac{1}{4}$ . Note that in the absence of temporal correlations, i.e.,  $\theta=0$ , the correction term to the vertex in Eq. (2.29b) vanishes as required by Galilean invariance.

From Eqs. (2.29), the fixed points can be determined by solving the flow structure in  $(U_0, U_\theta)$  space as in Sec. II B. The overall picture of the flows as a function of  $d'$ ,  $\rho$ , and  $\theta$  is similar to the case of spatial correlation only (see Fig. 3). Again there is a region in which white noise dominates. The boundary of this region is given by the stability of  $U_\theta$  in (2.29c), i.e.,

$$z_w(d')(1 + 2\theta) - 2\chi_w(d') - d' + 2\rho = 0.$$

Using Eqs. (2.24) for  $z_w$  and  $\chi_w$ , the boundary of this region for  $\rho=0$  is given by

$$\theta_c(d') = \frac{d'}{2} \frac{d' - 2}{d'^2 + 4d' - 8}. \quad (2.30)$$

Beyond this region,  $U_\theta$  becomes relevant; we must have (see Appendix A)

$$z(1 + 2\theta) - 2\chi - d' + 2\rho = 0 \quad (2.31)$$

for Eq. (2.29c) to hold at a fixed point. But unlike the case of spatial correlation, no simple expression for the exponents can be obtained because of the absence of Galilean invariance (and hence the loss of the exponent identity  $\chi + z = 2$ ). If we ignore the correction to the exponent identity in Eq. (2.29b), then Eq. (2.31) along with the exponent identity would result in the following expression for the exponents

$$z^*(\rho, \theta, d') = 2 - \frac{d'_c(\rho, \theta) - d'}{3 + 2\theta}, \quad (2.32a)$$

$$\chi^*(\rho, \theta, d') = \frac{d'_c(\rho, \theta) - d'}{3 + 2\theta}, \quad (2.32b)$$

where  $d'_c(\rho, \theta) = 2 + 2\rho + 4\theta$  is as given before. However, for large  $\theta$  we expect  $z(\rho, \theta, d')$  and  $\chi(\rho, \theta, d')$  to deviate significantly from  $z^*$  and  $\chi^*$ ; so the exponents should instead be obtained numerically by solving for the fixed point of the flow equations. As discussed in the case of spatial correlations, absence of a fixed point just below the upper critical dimension makes it impossible to con-

struct a systematic perturbation expansion for the fixed point. Also, lack of Galilean invariance implies that we cannot obtain any exact exponents in the presence of temporal correlations. For  $d'=1$  the one-loop recursion relations do provide us with an accessible fixed point. Although the results will not be systematic, to gain insight into the role of temporal correlations we shall examine the case  $\rho=0$  in some detail. For  $d'=1$  the recursion relations,

$$\begin{aligned} \frac{dU_\theta}{dl} &= U_\theta \left[ (1+4\theta) - \frac{3+2\theta}{4} U_0 \right. \\ &\quad \left. - U_\theta \sec(\pi\theta)(1+2\theta) \frac{3+10\theta}{4} \right], \\ \frac{dU_0}{dl} &= U_0 - \frac{1}{2} U_0 U_\theta \sec(\pi\theta)(1+2\theta) \frac{1+8\theta}{4} \\ &\quad + U_\theta^2 \sec(2\pi\theta) \frac{1+4\theta}{4}, \end{aligned}$$

are obtained from Eqs. (2.29) after eliminating  $z$  and  $\chi$ . A stable fixed point in the physical region (i.e.,  $U_0 \geq 0$ ,  $U_\theta \geq 0$ ) is found for  $0 \leq \theta < \frac{1}{4}$ ; the resulting exponents  $z(\theta)$  and  $\chi(\theta)$  are plotted. As shown in Fig. 5, the exponents increase for a range of  $\theta > \theta_c(d'=1) = \frac{1}{6}$ ; but then they turn around and rapidly approach the values  $z^*(\theta)$  and  $\chi^*(\theta)$  given by Eqs. (2.32) as  $\theta \rightarrow \frac{1}{4}$ . Beyond  $\theta = \frac{1}{4}$ , no stable point in the physical region is found in  $(U_0, U_\theta)$  space.

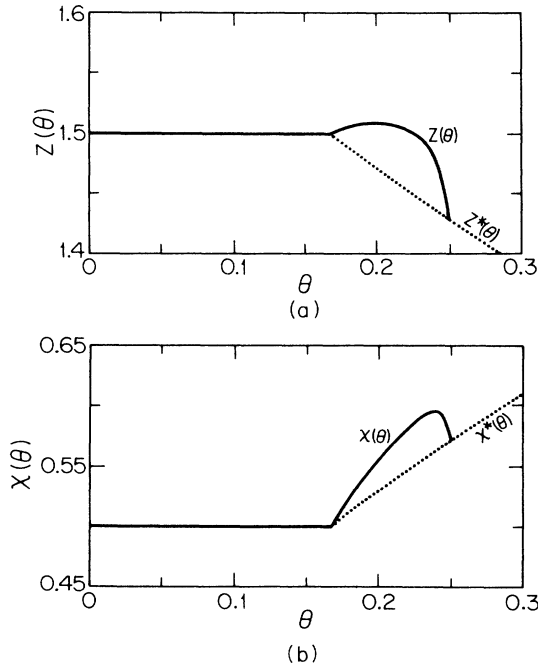


FIG. 5. (a) Dynamic exponent  $z$  and (b) roughening exponent  $\chi$  as a function of the exponent  $\theta$  for decay of temporal correlations, in  $d=2$  ( $d'=1$ ). The exponents are calculated to one loop for the choice of a spectral function  $D^*(\omega) = D_0^* + D^* \omega^{-2\theta}$ . There is no solution for  $\chi$  and  $z$  for  $\theta > \frac{1}{4}$ , indicating that form of  $D^*(\omega)$  is invalid for this range.

The behavior close to  $\theta = \frac{1}{4}$  is very suspicious, as physically there should be nothing special at  $\theta = \frac{1}{4}$ ; in particular Galilean invariance is still violated at this value. The source of such peculiar behavior is the infrared divergence of the integral for  $\tilde{D}_2^2$  which makes the last term in Eq. (2.29d) singular as  $\theta \rightarrow \frac{1}{4}$ . Going back to the derivation of  $\tilde{D}_2^2$  in Appendix D with  $\omega$  dependence included

$$\tilde{D}_2^2(\omega) = \frac{2}{\pi} \int_{-\infty}^{\infty} dz \frac{D \left[ 1, \omega_0 z + \frac{\omega}{2} \right] D \left[ 1, \omega_0 z - \frac{\omega}{2} \right]}{(1+z^2)^2}. \quad (2.33)$$

Using  $D(k, \omega) = D(\omega) \sim \omega^{-2\theta}$ , we find the leading  $\omega$  dependence of  $\tilde{D}_2^2(\omega)$  to be

$$\tilde{D}_2^2(\omega) = \tilde{D}_2^2(0) + O(\omega^{1-4\theta}) \quad \text{for } \theta \neq \frac{1}{4}.$$

An additional component of the spectral density function is generated under RG. It becomes "nonignorable" as  $\theta \rightarrow \frac{1}{4}$ . The fixed function is of the form  $D^*(\omega) = D_0 + D_1 \omega^{-2\theta_1} + D_2 \omega^{-2\theta_2}$ , where  $\theta_2 = 2\theta_1 - \frac{1}{2}$ . However with this new form, even more components are generated from the contractions  $\langle D_1 D_2 \rangle$  and  $\langle D_2 D_2 \rangle$ . By simple power counting, the contraction between  $D_i \omega^{-2\theta_i}$  and  $D_j \omega^{-2\theta_j}$  terms is

$$\langle D_i(\omega) D_j(\omega) \rangle = A(i, j) D_i D_j \omega^{1-2\theta_i-2\theta_j} + B(i, j) D_i D_j,$$

where  $A(i, j)$  and  $B(i, j)$  are integration constants. We can denote the new power generated in the same form,  $\omega^{-2\theta_{i+j}}$ , with  $\theta_{i+j} = \theta_i + \theta_j - \frac{1}{2}$ . If the most divergent part of  $D(\omega \rightarrow 0)$  is characterized by  $\omega^{-2\theta}$  then terms generated by RG are  $\omega^{-2\theta_n}$  with  $\theta_n = n\theta - (n-1)/2$ , and the fixed function is of the form  $D^*(\omega) = D_0^* + \sum_n D_n^* \omega^{-2\theta_n}$ . The number of divergent terms  $M(\theta)$  in the sum is the largest  $n$  for which  $\theta_n > 0$ , i.e.,

$$M(\theta) = \text{int} \left[ \frac{1}{1-2\theta} \right]. \quad (2.34)$$

As  $\theta$  increases from 0 to  $\frac{1}{2}$ , a new divergent term is added to the fixed function whenever  $\theta_n(\theta^*) = 0$ , where the special values  $\theta^*$ 's are

$$\theta^* = \frac{n-1}{2n} = 0, \frac{1}{4}, \frac{2}{6}, \frac{3}{8}, \frac{4}{10}, \dots$$

So the unphysical behavior obtained close to  $\theta = \frac{1}{4}$  is a reflection of emergence of the next divergent term in the fixed function  $D^*(\omega)$ .

Obviously, the RG flow space must be expanded for an improved treatment. The relevant integral for the noise contraction is computed in Appendix F; the coefficients  $A(i, j)$  and  $B(i, j)$  are given in Eq. (F2), and

$$A(i, j) = \frac{4}{\pi} \frac{\sin(\pi\theta_i) \sin(\pi\theta_j)}{\sin(\pi\theta_{i+j})} \frac{\Gamma(1-2\theta_i) \Gamma(1-2\theta_j)}{\Gamma(1-2\theta_{i+j})},$$

$$B(i, j) = (1+2\theta_i+2\theta_j) \sec[\pi(\theta_i+\theta_j)],$$

for  $\theta_{i+j} \neq 0$ . The two terms conspire to give  $\ln(\omega)$  when  $\theta_{i+j} = 0$  as in Eq. (F3).

Incorporating these results, we try a fixed function of the form

$$D_\theta(\omega) = D_0 + \sum_{n=1}^{N_{\max}} \pi D_n \frac{(\omega/\omega_0)^{-2\theta_n} - (1+2\theta_n)\sec(\pi\theta_n)}{\Gamma(1-2\theta_n)\sin(\pi\theta_n)},$$

with  $\theta_n = n\theta - (n-1)/2$  and the value of the cutoff  $N_{\max}$  will be discussed later. (Note that this form has the desired logarithms built in when  $\theta_n = 0$ .) The recursion relations Eq. (2.28) become

$$\frac{dv}{dl} = v \left[ z - 2 - \frac{d'-2}{4d'} U_0 \right],$$

$$\frac{d\lambda}{dl} = \lambda \left[ \chi + z - 2 - \frac{1}{2d'} \left[ \sum_{n=1}^{N_{\max}} \pi U_n \frac{(2\theta_n)(1+2\theta_n)\sec(\pi\theta_n)}{\Gamma(1-2\theta_n)\sin(\pi\theta_n)} \right] \right]$$

$$= \lambda \left[ \chi + z - 2 - \frac{1}{d'} \left[ \sum_{n=1}^{N_{\max}} U_n \Gamma(2+2\theta_n) \right] \right],$$

$$\frac{dU_1}{dl} = U_1 [z(1+2\theta) - 2\chi - d'],$$

$$\frac{dU_n}{dl} = U_n [z(1+2\theta_n) - 2\chi - d'] + \sum_{\substack{i,j=1 \\ (i+j=n)}}^{N_{\max}} U_i U_j,$$

$$\frac{dU_0}{dl} = U_0(z - 2\chi - d') + \frac{U_0^2}{4} + 4z\theta \sum_{n=1}^{N_{\max}} U_n(1+2\theta_n)\Gamma(2\theta_n)$$

$$+ 2[z(1+2\theta) - 2\chi - d'] \sum_{n=1}^{N_{\max}} U_n(n-1)(1+2\theta_n)\Gamma(2\theta_n)$$

$$+ \sum_{i,j=1}^{N_{\max}} U_i U_j \Gamma(2\theta_i)\Gamma(2\theta_j) \left[ (1+2\theta_i+2\theta_j) \frac{\cos(\pi\theta_i)\cos(\pi\theta_j)}{\cos[\pi(\theta_i+\theta_j)]} - (1+2\theta_i)(1+2\theta_j) \right],$$

where the identity  $\Gamma(z)\Gamma(1-z) = \pi/\sin(\pi z)$  is used, and  $U_i \equiv K_d \lambda^2 D_i / v^3$  as before.

The condition  $dU_1/dl = 0$  implies  $2\chi + d' = z(1+2\theta)$  for  $\theta > \theta_c$ . So

$$\frac{dU_n}{dl} = U_n z(2\theta_n - 2\theta) + \sum_{i+j=n} U_i U_j = U_n z(2\theta - 1)(n-1) + \sum_{i+j=n} U_i U_j.$$

By setting  $dU_n/dl = 0$ , it is easy to verify that

$$U_n = [z(1-2\theta)]^{-n+1} U_1^n.$$

Hence we can describe the fixed function  $D^*(\omega)$  by two parameters  $D_0^*$  and  $D_\theta^*$  as

$$D_\theta(\omega) = D_0^* + \sum_{n=1}^{N_{\max}} \frac{\pi(D_\theta^*)^n}{[z(1-2\theta)]^{n-1}} \left[ \frac{(\omega/\omega_0)^{-2\theta_n} - (1+2\theta_n)\sec(\pi\theta_n)}{\Gamma(1-2\theta_n)\sin(\pi\theta_n)} \right]. \tag{2.35}$$

The exponents  $\chi$  and  $z$  are calculated from

$$z = 2 - \frac{2-d'}{4d'} U_0^*, \tag{2.36a}$$

$$\chi = \frac{2-d'}{4d'} U_0^* + \frac{1}{d'} \sum_{n=1}^{N_{\max}} U_n^* \Gamma(2+2\theta_n), \tag{2.36b}$$

with

$$U_n^* = \frac{(U_\theta^*)^n}{[z(1-2\theta)]^{n-1}}, \quad 2\theta_n = 1 - n(1-2\theta), \tag{2.36c}$$

where the fixed points  $U_0^*$  and  $U_\theta^*$  are found from the flow equations

$$\frac{dU_\theta}{dl} = U_\theta[z(1+2\theta) - 2\chi - d'] , \quad (2.36d)$$

$$\begin{aligned} \frac{dU_0}{dl} = & U_0(z - 2\chi - d') + \frac{U_0^2}{4} + 4z\theta \sum_{n=1}^{N_{\max}} U_n(1+2\theta_n)\Gamma(2\theta_n) \\ & + 2[z(1+2\theta) - 2\chi - d'] \sum_{n=1}^{N_{\max}} U_n(n-1)(1+2\theta_n)\Gamma(2\theta_n) \\ & + \sum_{i,j=1}^{N_{\max}} U_i U_j \Gamma(2\theta_i)\Gamma(2\theta_j) \left[ (1+2\theta_i+2\theta_j) \frac{\cos(\pi\theta_i)\cos(\pi\theta_j)}{\cos[\pi(\theta_i+\theta_j)]} - (1+2\theta_i)(1+2\theta_j) \right] . \end{aligned} \quad (2.36e)$$

The terms that seem to diverge as  $\theta_n \rightarrow 0$  in the last equation cancel each other; and Eqs. (2.36) can easily be solved numerically in the range  $0 \leq \theta < \frac{1}{2}$  once  $N_{\max}$  is defined.

From the preceding discussion it seems as if the sum should be unbounded since terms with arbitrarily large positive powers are generated. This might be a serious problem because the frequency integrals contributing to one-loop propagator and vertex correction will have ultraviolet divergence if the full form of  $D^*(\omega)$  is used for the entire range  $0 \leq \omega \leq \infty$ ; a cutoff must be made as  $D^*(\omega)$  is really only the behavior in the  $\omega \rightarrow 0$  limit. On the other hand, the coefficients of the higher-order terms are suppressed by a factor of  $1/\Gamma(2n\theta)$ ; as a result the exponents should not depend too sensitively on the upper cutoff.

Equations (2.36) are solved numerically for various  $N_{\max}$  at  $d'=1$ , and the resulting exponents  $z(\theta)$  and  $\chi(\theta)$  are shown in Figs. 6(a) and 6(b). We observe that in the region with  $M(\theta)$  divergent terms as given by Eq. (2.34),

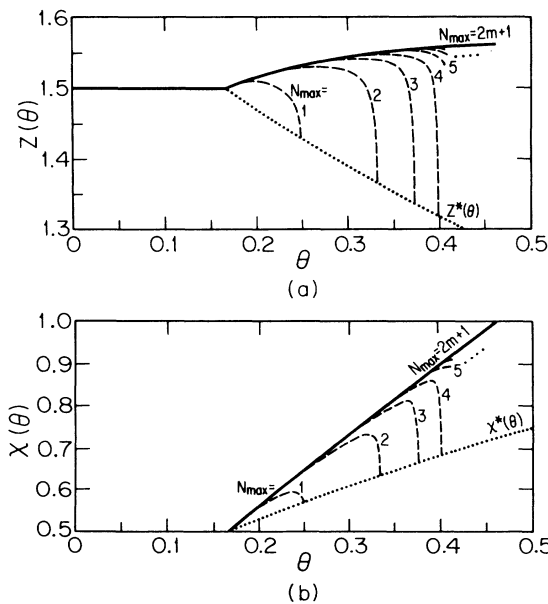


FIG. 6. Some exponents as in Fig. 5 calculated by including more and more powers, generated by renormalization, in the spectral function  $D^*(\omega)$ . The exponents are found to rapidly converge upon including more powers.

at least  $M(\theta)$  terms are necessary to find fixed points and exponents at all; beyond that the convergence of the series is rather fast.  $N_{\max}$  can be pushed to  $2M(\theta)+1$  giving exponents with an accuracy of better than 0.1% before Eqs. (1.36) become problematic. Using this upper cutoff, we find that  $\chi(\theta)$  calculated can be fitted to a straight line

$$\chi(\theta) = 1.69\theta + 0.22 ,$$

and the corresponding expression for  $z(\theta)$  is obtained from the fixed point condition for  $U_\theta$  in Eq. (2.36c)

$$z(\theta) = \frac{2\chi(\theta) + 1}{1 + 2\theta} .$$

The calculation becomes increasingly difficult to carry out as  $\theta \rightarrow \frac{1}{2}$  because  $N_{\max} > M(\theta) \sim (1-2\theta)^{-1} \rightarrow \infty$ . In any case, the results obtained for  $d'=1$  have  $\chi$  exceeding 1 at  $\theta=0.46$ ; so the theory is not valid for  $\theta$  close to  $\frac{1}{2}$ , since  $\chi > 1$  would necessitate including higher powers of  $\nabla h$  in Eq. (1.2) (as argued earlier).

Finally, we look at the situation for  $\theta \geq \frac{1}{2}$ : From simple power counting (see results of  $\langle D_i D_j \rangle$  contraction in Appendix F), we see that the situation is quantitatively changed for  $\theta > \frac{1}{2}$ , because increasingly more divergent terms are generated by RG, giving the fixed function an essential singularity at  $\omega=0$ . As a consequence no stable surface can survive in any dimension and higher powers of  $\nabla h$  are essential.

The case of  $\theta = \frac{1}{2}$  corresponding to the ubiquitous  $1/\omega$  noise is special:  $\langle DD \rangle$  contraction does not generate any new term; so the fixed function has the simple form  $D(\omega) = D_\theta/\omega$ . However, the renormalization procedure outlined in Sec. II B breaks down here because the frequency integrals in one-loop calculations also have infrared divergencies for  $\theta \geq \frac{1}{2}$ . This divergence may be tamed by switching the role of space and time in the RG treatment; i.e., do the coarse graining, averaging in time, and perform integrations over internal momenta. Such a treatment is rather involved and will not be dealt with here. Nevertheless it may be worthwhile to solve for the behavior at  $\theta = \frac{1}{2}$  to see how the system switches from a well behaved region for  $\theta < \frac{1}{2}$  to the unstable region when  $\theta > \frac{1}{2}$ . In addition we may gain some insight into the nature of  $1/\omega$  noise.

### III. DIRECTED PATHS IN RANDOM MEDIA

Understanding the statistical mechanics of disordered systems has proved to be a most challenging problem.<sup>14</sup> The complexity of dynamics of relaxation in these systems is partly due to the pinning of domain walls by impurities.<sup>15,16</sup> A domain wall of characteristic size  $L$  is expected to be subject to pinning barriers of typical energy growing as  $L^\omega$ . Another consequence of impurities is an anomalous roughening of domain walls such that typical height fluctuations grow as  $L^\chi$  with an exponent  $\chi$  larger than the "ideal-surface" value of  $(3-d)/2$  calculated in Sec. II. As a prototype, the interface of the Ising model in two dimensions has been the subject of extensive studies, both analytical<sup>9,17</sup> and numerical.<sup>18-20</sup>

Numerical simulations in  $d=2$  are performed on a discrete interface described by  $x(t)$  ( $x, t$  both integers);

$$W(x, t) = \int_{(0,0)}^{(x,t)} Dx'(t') \exp \left\{ - \int_0^t dt' \left[ \frac{\nu}{2} \left( \frac{dx'}{dt'} \right)^2 + \mu(x', t') \right] \right\}, \quad (3.1)$$

where  $\nu$  is an effective line tension, and  $\mu(x, t)$  represents the effects of impurities on the interface crossing the point  $(x, t)$ . Clearly  $W(x, t)$  satisfies the differential equation

$$\frac{\partial W}{\partial t} = \nu \frac{\partial^2 W}{\partial x^2} + \mu(x, t), \quad (3.2)$$

which is the same as Eq. (1.3) for  $d'=1$ . This mapping thus relates the free-energy profile [ $f(x, t) = -\ln W$ ] of the static problem of an interface in a random environment, to the dynamics of the Burgers equation. The fixed random energies  $\mu(x, t)$  are mapped onto the stochastic noise acting on Eq. (1.3). It also follows that the roughening exponent ( $\delta x \sim t^\chi$ ) is related to the dynamic exponent of the Burgers equation via  $\chi = 1/z$ . For random bonds  $\mu(x, t)$  are independent random variables, and the white-noise result  $z = \frac{3}{2}$  translates into the numerically observed<sup>18,19</sup> value of  $\frac{2}{3}$  for  $\chi$ . In the case of random fields<sup>21</sup> the effective energy cost of an interface crossing at height  $x$  is made up of the sum of random fields in the same column  $t$ , i.e.,

$$\mu(x, t) = \sum_{x'(<x)} R(x', t), \quad (3.3)$$

where the fields  $R(x', t)$  are now independently distributed. This leads to long-range (spatial) correlations in the noise described by<sup>21</sup>  $\rho = 1$ . As Fig. 4 indicates,  $\rho = 1$  leads to a dynamic exponent  $z = 1$  in  $d' = 1$ , again in support of numerical simulations indicating  $\chi = 1$  in the presence of random fields.<sup>16</sup> We can also consider impurities interacting with the interface through a long range potential falling off algebraically, i.e.,

$$\mu(x, t) = \sum_{x'(<x)} R(x', t) / |x - x'|^{1-\rho}. \quad (3.4)$$

This is clearly a discrete limit of Eq. (2.3), and interpolates between random bond and random field cases as  $\rho$  is

i.e., overhangs are ignored. A transfer-matrix method is then usually employed to obtain the ground states and statistics of the problem. The first set of simulations were performed in the presence of random field impurities,<sup>16</sup> and strongly suggested the exponents  $\chi = \omega = 1$  (indicating  $d = 2$  as the lower critical dimension of the random field Ising model). Recently Huse and Henley<sup>18</sup> performed similar simulations in the presence of random bonds and discovered anomalous exponents  $\chi = \frac{2}{3}$  and  $\omega = \frac{1}{3}$  (compared with  $\chi = \frac{1}{2}$  and  $\omega = 0$  for the ideal surface). These results are exact as can be shown from a number of analytic approaches such as the replica method.<sup>17</sup> A particularly elegant demonstration is due to Huse, Henley, and Fisher.<sup>9</sup> Consider the partition sum  $W(x, t)$  of the weights of all paths connecting the origin  $(0, 0)$  to the point  $(x, t)$ . In the continuum limit,

varied from 0 to 1. The roughening exponent  $\chi$  for this generalized model is again read off easily from Fig. 4, and interpolates from  $\frac{2}{3}$  to unity. A related model, in the context of anticorrelated impurities, was recently considered by Nattermann.<sup>12</sup>

An interesting question concerns the fluctuations in the shape of a domain wall as it moves through the random environment. The optimal paths in fact form a hierarchical structure reminiscent of river basins, as depicted in Fig. 7. In these figures one end of an interface is pinned at the apex of each triangle, while the other end is moved along the base. The different figures correspond to different values of  $\rho$  in the interval 0 to 1. These pictures show qualitatively how the tree structure changes from the case of random fields ( $\rho = 1$ ) to random bonds ( $\rho = 0$ ). We have not attempted to make a quantitative analysis of these patterns.

A few words on the numerical procedure are appropriate here. The paths in Fig. 7 are non-Markovian in nature, in the sense that the impurities at large  $t$  influence and modify the optimal path at small  $t$ . However, the energy profile  $E(x, t)$  of optimal paths connecting the apex to the point  $(x, t)$  evolves in a Markovian way [as in Eq. (3.2)]. Thus rather than updating a single optimal path, one updates a whole energy profile  $E(x, t)$ . This involves keeping  $O(t_{\max})$  numbers in the memory, and the computation time grows as  $t_{\max}^2$ . The end point of the optimal paths can then be obtained from the optimum of  $E(x, t_{\max})$ . To generate the complete shape of the optimal paths as in Fig. 7 is slightly more complicated. This is done by keeping in the memory at each step the direction  $v(x, t)$  of the local optimal path to  $(x, t)$ . Once the calculation has proceeded to  $t_{\max}$ , this information can be used to draw an optimal path backward. The memory requirement for this case grows as  $t_{\max}^2$ . The total number of possible paths, of course, grows exponentially in  $t_{\max}$ , but the transfer-matrix procedure allows us

to obtain information regarding the optimal paths in polynomial time.

The interface problems in three and higher dimensions are considerably more complicated. There is no mapping to a Burgers-type equation, and a numerical transfer-matrix calculation has to follow the evolution of a string. The memory requirements and calculational times now grow exponentially with the interface width. We have in fact carried out such a calculation,<sup>22</sup> but due to the small sizes of the interfaces that are tractable the results are not very reliable. Another possible generalization is to examine linear defects in higher dimensions. This problem, by construction, corresponds to the generalization of Eq. (1.1) to higher dimensions  $d$ . Physically we may encounter this situation for directed polymers (as in polyelectrolytes) moving in a random and quenched gel matrix.<sup>8</sup>

In the absence of impurities, the polymer executes a random walk in the transverse direction, and as a result typical transverse fluctuations  $|\mathbf{x}|$  scale with the length  $t$  of the directed polymers as  $|\mathbf{x}| \sim t^\nu$  with  $\nu = \frac{1}{2}$ . It is clear that in general the exponent  $\nu$  is related to the dynamic exponent of the corresponding the Burgers equation via  $\nu = 1/z$ . A nontrivial  $z$  therefore corresponds to anomalous transverse fluctuations. For the rest of this section we will concentrate on uncorrelated random impurities

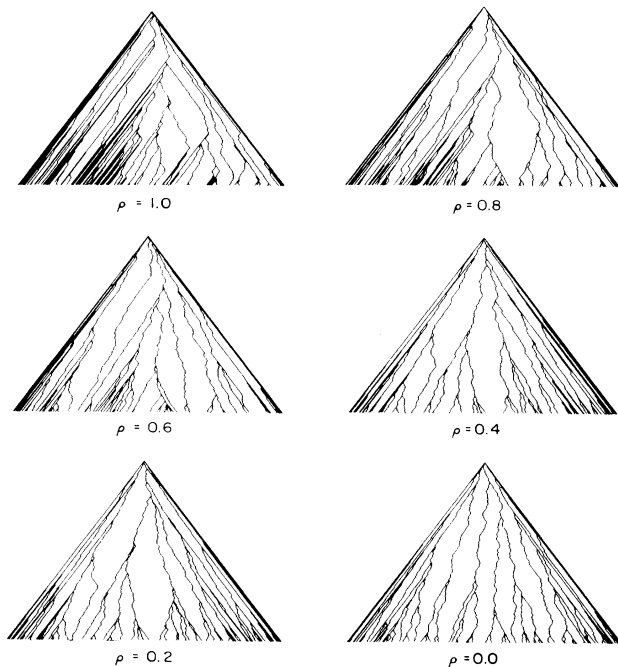


FIG. 7. Optimal paths of 500 bonds along diagonals of a square connecting the apex to various points on the base. The bonds are all random variables, with correlations in horizontal strips, decaying with an exponent  $\rho$ . Different figures correspond to different values of  $\rho$ , varied from 1.0 (upper left) to 0.0 (lower right) in steps of 0.2. As explained in Sec. III,  $\rho=0$  corresponds to random bonds, while  $\rho=1$  represents random fields, for an Ising model.

$\mu(\mathbf{x}, t)$ . As discussed in Sec. II the renormalization flows only result in a finite strong coupling fixed point in  $d=2$ . For  $d=3$  impurities are marginally relevant and the flow is to infinity. Similarly in  $d=4$  the flows indicate a transition to strong-coupling behavior for sufficiently strong randomness. Therefore although in dimensions  $d \geq 3$  the RG flows suggest an anomalous exponent  $z$ , the actual exponent is not reached by perturbative schemes, and other means have to be employed.

We carried out extensive numerical simulations of optimal directed paths in dimensions  $d=2, 3$ , and 4, on a Cray XMP computer.<sup>8</sup> Details of the procedure have been discussed elsewhere, and are straightforward generalizations of the transfer-matrix procedure to higher dimensions.<sup>8</sup> For each realization of randomness typical transverse fluctuations  $|\mathbf{x}|$ ; and energy fluctuations  $\Delta E$  of the optimal paths were calculated as a function of  $t$ . The results after averaging over many realizations of randomness, were fitted to power laws  $\langle |\mathbf{x}| \rangle \sim t^\nu$  and  $\langle \Delta E \rangle \sim t^\omega$ . For  $d=2$  the predicted exponents  $\nu = \frac{2}{3}$  and  $\omega = \frac{1}{3}$  were recovered. For higher dimensions we indeed observed nontrivial scaling with estimated exponents  $\nu = 0.62 \pm 0.04$  and  $\omega = 0.33 \pm 0.02$  in  $d=3$ , and  $\nu = 0.64 \pm 0.07$  and  $\omega = 0.41 \pm 0.04$  in  $d=4$ .

Based on these results we conjectured<sup>8</sup> that the exponents  $\nu = \frac{2}{3}$  and  $\omega = \frac{1}{3}$  may in fact be valid in all dimensions, i.e., superuniversal. Although this is consistent with our simulations, it seems not to be supported by simulations on the related interface problem to be discussed in Sec. IV.<sup>13</sup> Since we have not clearly identified a fixed point for the strong-coupling behavior, there could still be questions regarding the uniqueness of the strong-coupling exponents. In any case, all numerical simulations so far support two important conclusions of the renormalization-group procedure. First they confirm the existence of a new behavior with  $z \neq 2$  for strong randomness. Second all simulations agree with the exponent identity  $\chi + z = 2$  which follows from Galilean invariance (note that  $\omega = \chi/z$  for the directed-polymer problem). Recently Derrida and Spohn<sup>23</sup> have solved exactly the problem of directed polymers on a Cayley tree. On a tree no exponent  $\nu$  can be defined; however, they demonstrate a phase transition as a function of disorder, and for strong disorder they find  $\Delta E \sim \ln t$  (i.e.,  $\omega=0$ , although the fluctuations are still anomalous). Assuming that as usual the Cayley-tree results apply to Euclidean lattices as  $d \rightarrow \infty$ ; the conclusion is that the anomalous  $\nu$  decreases to  $\frac{1}{2}$  as  $d \rightarrow \infty$ ; but that logarithmic corrections remain at  $d = \infty$ .

#### IV. DYNAMICS OF GROWING SURFACES

The patterns formed in growth processes have been a constant source of fascination and scientific inquiry.<sup>24</sup> In many cases the patterns are due to inherent instabilities of a growth front controlled by an underlying diffusion mechanism. Yet it is instructive to examine a simpler type of growth exemplified by a vapor-deposition process, where the growth rate is locally determined by the flux of particles arriving ballistically at the surface. Although there are no instabilities in the usual sense, this process

leads to a variety of columnar structures.<sup>25</sup> The origin of these structures can be traced back to nonlinearities that are dynamically generated in the growth process. In fact the simplest nonlinear equation describing the evolution of the surface profile  $h(\mathbf{x}, t)$  moving with an average velocity  $v_0$  is<sup>5</sup>

$$\frac{\partial h}{\partial t} = v\nabla^2 h + \frac{\lambda}{2}(\nabla h)^2 + \eta(\mathbf{x}, t) + v_0. \quad (4.1)$$

Clearly in a coordinate frame moving with the interface, fluctuations around the average position  $h(x, t) \rightarrow h(x, t) - v_0 t$  are described by Eq. (1.2).

The first term in the preceding equation describes the relaxation of the interface by a surface tension  $\nu$ , for example, by evaporation and readsorption of particles on the surface. Such relaxation can be obtained by considering a "capillary-wave" Hamiltonian  $H_{CW} = \int d^{d-1}x (\nabla h)^2$ ; and constructing the corresponding Langevin equation.<sup>1,2</sup> This is in fact the simplified model studied by Edwards and Wilkinson,<sup>26</sup> and predicts that the growing interface behaves as a "free surface;" i.e., for  $d > 3$  the interface is flat while for  $d \leq 3$  typical roughness at size  $L$  scales as  $L^\chi$  with  $\chi = \chi_0 = (3-d)/2$ . Relaxation of fluctuations is also described by the dynamic exponent  $z_0 = 2$ . According to the linear equation the shape of the profile is symmetric about the average position [due to the  $h(x) \rightarrow -h(x)$  symmetry]. This is clearly not true for a typical growth profile from which it is usually possible to identify the growth direction. This by itself leads us to suspect nonlinear terms that break this symmetry.

To see how the nonlinear term in Eq. (4.1) originates, consider growth by addition of discrete spherical particles of diameter  $d$  to a surface as in Fig. 8. It is clear that the growth direction is always locally normal to the surface. Consequently, as Fig. 8 demonstrates the vertical change  $\delta h$  is given by  $\delta h = d/\cos\theta = d[1 + (\nabla h)^2]^{1/2}$ . The local slope  $\nabla h$  therefore appears in the growth equations in a nonlinear and nonsymmetric form. In a continuum limit it is clear that the slope  $\nabla h$  is *parallel transported* during growth, and hence  $\mathbf{v} = -\nabla h$  satisfies a Navier-Stokes equation as in Eq. (1.1). The relation to the Burgers equation and the necessity for the nonlinear term now becomes apparent. Also it is clear that the parameter  $\lambda$  in Eq. (4.1) has to be proportional to the average velocity  $v_0$ ; i.e., the nonlinearity is dynamically generated.

The need for nonlinearities in a description of surface dynamics had been recognized earlier by Bausch *et al.*<sup>27</sup> for a stationary interface, and in the context of columnar growth by Ramanlal and Sander.<sup>28</sup> It is instructive to first examine the relaxation of an initially rough surface

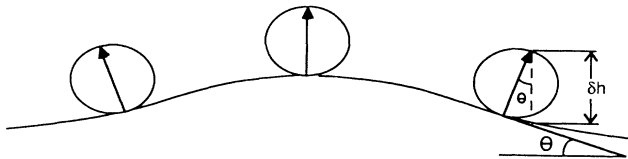


FIG. 8. Growth by addition of spherical particles. It can be seen that growth occurs always normal to the interface so that the local tangent vector is parallel transported.

deterministically, i.e., according to Eq. (4.1) with  $\eta(\mathbf{x}, t) = 0$ . After mapping to a diffusion equation as in Eq. (1.3), we can solve exactly the evolution of any initial pattern  $h(x, t = 0) = h_0(x)$ , and conclude

$$h(\mathbf{x}, t) = v_0 t + \frac{2\nu}{\lambda} \ln \left[ \int_{-\infty}^{\infty} d\xi \frac{1}{(4\pi\nu t)^{d'/2}} \times \exp \left[ -\frac{(x-\xi)^2}{4\nu t} + \frac{\lambda}{2\nu} h_0(\xi) \right] \right]. \quad (4.2)$$

The inside integral can be evaluated by the saddle-point method for small surface tensions, i.e.,  $\nu \rightarrow 0$  (Burgers shows that<sup>3</sup> similar results are obtained in the long-time limit  $t \rightarrow \infty$ ). After maximizing the integrand and taking a logarithm, the solution is found to be composed of paraboloid segments  $h_n = A_n - (x - \xi_n)^2 / 2\lambda t$  joined together by discontinuities in  $\nabla h$ . For a finite  $\nu$  the discontinuity is somewhat smoothed out. A typical one-dimensional growth pattern is sketched in Fig. 9, together with the asymptotic form of  $v = -\partial h / \partial x$ . Such patterns are quite commonly encountered in nature in geological stratifications, successive layers of snow drifts, etc. The relation between parabolic patterns and shock waves of the Burgers equation is also apparent from this figure.

Further evolution of the pattern proceeds through the larger paraboloid segments growing at the expense of smaller ones, and parallels the evolution of shock waves which may be more familiar. In one dimension it is easy to calculate the scaling of the average size of these paraboloids with time. In the saddle-point minimization we can look at some point  $x$ , and ask how far it is from the center  $\xi_n$  of the paraboloid to which it belongs. Moving to  $\xi$  reduces the exponent by  $(x - \xi)^2 / 4\nu t$ . This reduction will be tolerated if  $h_0(\xi)$  is sufficiently large. If the initial profile is rough (i.e.,  $P(h_0(\xi)) \sim \exp[-(K/2) \int dx (dh/dx)^2]$ ),  $h_0(\xi)$  undergoes a random walk and is expected to fluctuate on average as much as  $|x - \xi|^{1/2}$ . Balancing the two terms we find  $|x - \xi_n| \sim t^{2/3}$ ; i.e., typical widths of the paraboloid grow as  $t^{2/3}$ , and typical heights as  $t^{1/3}$ . These exponents are remarkably the same as  $1/z$  and  $\chi/z$  for the stochastic equation. Note, however, that in higher dimensions a profile distributed according to  $P(h_0(\xi)) \sim \exp[-(K/2) \int d^{d-1}x (\nabla h)^2]$  is already flat, and the typical curvature of paraboloids decreases as  $1/t$  without any appreciable change in their extent. Deterministic growth equations with a general  $|\nabla h|^\beta$  replacing  $(\nabla h)^2$  in Eq. (4.1) have also been recently examined from the scaling point of view.<sup>29</sup>

For the stochastic growth problem we can now use the results obtained in Sec. II. For example, in the absence of any long-range correlations in the local growth factors  $\eta(\mathbf{x}, t)$  (i.e., for  $\theta = \rho = 0$ ), we expect in  $d = 2$  a nontrivial growth characterized by  $\chi = \frac{1}{2}$  and  $z = \frac{3}{2}$  due to relevance of nonlinearities. In  $d = 3$ , again nonlinearities are

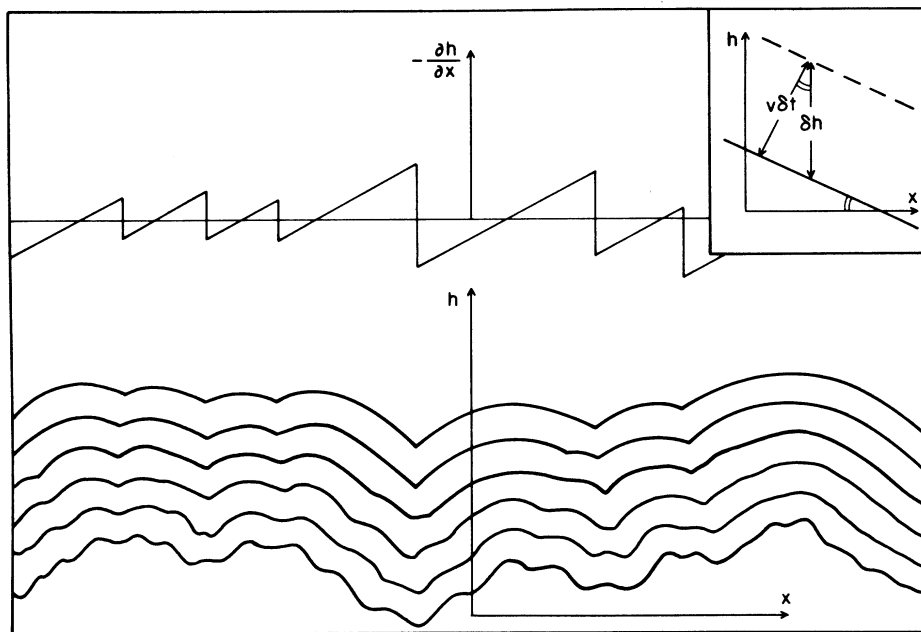


FIG. 9. Successive layers of an interface relaxing to a flat configuration by a deterministic growth mechanism similar to Eq. (4.1). The relaxation occurs via paraboloid segments joined together at cusps. The gradient of the surface profile evolves according to the Burgers equation, and develops shock fronts corresponding to the cusps.

relevant and by analogy with the directed polymer problem nontrivial exponents  $\chi \sim 0.4$  and  $z \sim 1.6$  are expected. In higher dimensions both trivial ( $\chi=0$ ,  $z=2$ ) and nontrivial exponents ( $\chi > 0$ ,  $z < 2$ ) are possible depending on the relative strengths of surface tension and nonlinear terms. We shall now compare these predictions with numerical simulations of growth.

Some of the earliest numerical results are due to Family and Vicsek<sup>30</sup> on a “ballistic deposition model,” which describes vapor deposition processes. New particles come down vertically and become part of the growing surface on impact with a surface particle (sideways sticking is allowed). Their simulations show<sup>30</sup> that initially the interface width grows with time as  $t^{0.30 \pm 0.02}$ , very close to our prediction of  $t^{\chi/z=1/3}$ . Eventually the width saturates to a value that scales with the interface size  $L$  as  $L^\chi$  with  $\chi = 0.42 \pm 0.02$ , not very different from the predicted value of  $\frac{1}{2}$ . The dynamic scaling form, i.e., width  $\sim L^\chi g(t/L^z)$ , was also observed by Plischke and Racz on the Eden model.<sup>31</sup> In the Eden model a surface site is selected at random, and one of the available neighboring sites is added to the cluster. The numerical estimate of  $z = 1.55 \pm 0.15$  is in excellent agreement with the prediction of  $\frac{3}{2}$  ( $\chi$  is fixed to  $\frac{1}{2}$  in simulations). Note that unlike diffusion-limited aggregates, both ballistic deposition and Eden growth lead to compact clusters, but the behavior of surface fluctuations is still interesting.

The fact that  $\chi$  takes the same value of  $\frac{1}{2}$ , as in the “free” interface, initially led to conjectures that  $\chi = \chi_0 = (3-d)/2$  in all dimensions.<sup>31,32</sup> This appeared to agree with simulations on small strips<sup>32</sup> for  $d=3$  and 4. However, because of the small sizes these results were not reliable, and we have seen that nonlinearities lead to a

different  $\chi$ . Since the publication of the original paper<sup>5</sup> on Eq. (4.1), various numerical and analytic studies have appeared that shed new light on growth problems, and some of these results will be briefly summarized here.

For  $d=2$  extensive numerical simulations on the Eden surface by Zabolitzky and Stauffer,<sup>33</sup> and on different ballistic deposition models by Meakin, Ramanlal, Sander, and Ball<sup>34</sup> (MRSB) and Plischke, Racz, and Liu<sup>35</sup> (PRL) quite convincingly confirm the exponents  $\chi = \frac{1}{2}$  and  $z = \frac{3}{2}$ . The small discrepancies between the earlier simulations<sup>30–32</sup> and theoretical predictions<sup>5</sup> are thus removed. MRSB (Ref. 34) provide a nice argument for the generation of the nonlinear term, starting from a discrete growth model. The model studied by PRL (Ref. 35) allows simultaneous deposition and evaporation of particles. They can then explicitly show that the nonlinear term is present because of the breaking of time-reversal symmetry. When the average deposition and evaporation rates are equal, time-reversal symmetry is restored and the nonlinear term vanishes.

MRSB also introduce a growth model which is in fact exactly solvable for  $d=2$  and leads to  $\chi = \frac{1}{2}$  and  $z = \frac{3}{2}$ . Yet another exactly solvable growth model in  $d=2$  has been introduced by Dhar<sup>36</sup> who also gets the same exponents. In conclusion essentially all theoretical and numerical simulations of growth for  $d=2$  indicate the presence of the nonlinear term and agree on the exponents  $\chi = \frac{1}{2}$  and  $z = \frac{3}{2}$ .

The situation in higher dimensions is less clear. The simulations of Zabolitzky and Stauffer<sup>33</sup> clearly rule out  $\chi = \chi_0$ , but cannot provide a definite answer for the asymptotic exponents. The lattice simulations of MRSB (Ref. 34); and off lattice simulations of Jullien and Mea-

kin,<sup>37</sup> give  $\chi \sim \frac{1}{3}$ . Wolf and Kertesz in a series of investigations<sup>13,38</sup> of Eden surfaces conclude  $\chi = 0.33 \pm 0.01$  in  $d = 3$  and  $\chi = 0.24 \pm 0.02$  in  $d = 4$ . They hence conjecture  $\chi = 1/d$  in  $d$  dimensions. This clearly differs from the conjecture of a superuniversal  $\chi = \frac{1}{2}$  based on our simulations of directed polymers.<sup>8</sup> As mentioned in Sec. IV, the polymer results are not inconsistent with  $\chi = 1/d$ , which is in fact a more appealing result as it goes to the free interface limit for  $d \rightarrow \infty$ , and thus can be connected with the result of Ref. 29 on a Cayley tree. Also a “proof” of superuniversality of  $\chi$  by McKane and Moore<sup>39</sup> does not really exclude this possibility. It is worth reemphasizing that all simulations reported so far agree on the validity of  $\chi + z = 2$  which follows from Galilean invariance.

It is hard to come up with physical problems where long-range correlations in the local growth probability may occur.<sup>40</sup> One possibility is relatively immobile impurities in the path of the interface that get trapped by it and impede further growth at that point. Another possible case is when there are charged ions that become part of the interface and effect further growth via the long range Coulomb interaction. It would be interesting to come up with such a model that is easy to simulate, yet violates the Galilean invariance. The breakdown of  $\chi + z = 2$  can then be probed in such a model.

#### ACKNOWLEDGMENTS

We have benefitted from conversations with S. Zalesky. This research was supported by the National Science Foundation (NSF) through Grant No. DMR-86-20386. One of us (M.K.) acknowledges support from the Alfred P. Sloan Foundation. One of us (E.M.) acknowledges support from the “Centro de Investigacion y Desarrollo” INTEVEP S. A. Venezuela.

#### APPENDIX A: EXPONENT IDENTITIES FROM NONRENORMALIZATION OF CORRELATED NOISE

The stable fixed points governing the scaling behavior, encountered in this paper, can be subdivided into the following two distinct categories.

(i) At the fixed point the noise is white with no correlations (e.g., region A in Fig. 3).

(ii) The noise at the fixed point is long-range correlated and characterized by the exponents  $\rho$  or  $\theta$  (e.g., region B in Fig. 3).

The second type of fixed point is in a sense simpler to handle since there is an exponent identity relating the exponents  $\chi$  and  $z$ . This exponent identity follows from nonrenormalization of correlated noise and is characteristic of long-range interactions.<sup>1</sup> The RG equations giving the corrections to  $D(\mathbf{k}, \omega)$  only produce analytic powers of  $k$  (spatial correlations), or higher nonanalytic powers of  $\omega$  (temporal correlations). This was shown explicitly in Sec. II at the one-loop order, and in fact holds at all orders. Hence the lowest nonanalytic powers of  $k$  or  $\omega$  in the noise spectrum  $D(\mathbf{k}, \omega)$  obtains no anomalous corrections from the integration of short wavelength modes. The scaling of this term therefore arises fully

from its “bare” dimension as in Eq. (2.7). At the fixed point, the scale invariance of this term, immediately leads to the *exact* exponent identity

$$2\rho - d' - 2\chi + (\theta + 1)z = 0. \quad (\text{A1})$$

For spatial correlations ( $\theta = 0$ ), the above identity, in addition to the identity that follows from Galilean invariance [Eq. (B6)] leads to the exponents  $\chi = 1 - (d' + 1 - 2\rho)/3$  and  $z = 1 + (d' + 1 - 2\rho)/3$  given in Eq. (2.26). These exponents are exact in region B, but the boundary of this region depends on the exponents  $z_w(d)$  and  $\chi_w(d)$  for white noise. Hence this boundary is only known within the one-loop approximation. The only exception is for  $d' = 1$ , where as discussed by FNS (Ref. 4) there is (with uncorrelated noise) a fluctuation-dissipation theorem<sup>41</sup> that ensures that  $\nu$  and  $D$  scale in the same way to all orders in perturbation theory. This immediately leads to  $\chi_w(1) = \frac{1}{2}$  and  $z_w(1) = \frac{3}{2}$ ; and allows us to obtain the exact exponents  $\chi$  and  $z$  for all  $\rho$  (as in Fig. 4). Although the exponent identities lead to the exact exponents, the position of the fixed point is only known perturbatively and is expected to change upon going to higher loop calculations.

#### APPENDIX B: CONSEQUENCES OF GALILEAN INVARIANCE

The Burgers equation has a Galilean invariance associated with looking at the fluid in a moving frame. Hence the transformation<sup>4</sup>

$$\mathbf{v}(\mathbf{x}, t) \rightarrow \mathbf{v}_0 + \mathbf{v}'(\mathbf{x} - \mathbf{v}_0 t, t) \quad (\text{B1})$$

is an exact symmetry of the equation (with  $\lambda = 1$ ). For the interface equation (1.2) this symmetry corresponds to the infinitesimal reparametrization

$$h' = h + \epsilon \cdot \mathbf{x}, \quad \mathbf{x} = \mathbf{x} + \lambda \epsilon t', \quad t = t', \quad (\text{B2})$$

which describes the tilting of the interface by a small angle  $\epsilon$ . The tilted surface to  $O(\epsilon)$  satisfies the equation

$$\frac{\partial h'}{\partial t'} = \nu \nabla'^2 h' + \frac{\lambda}{2} (\nabla' h')^2 + \eta(\mathbf{x} + \lambda \epsilon t', t'). \quad (\text{B3})$$

Clearly the deterministic equation is invariant under this transformation, while the stochastic equation is subject to a noise  $\eta'(\mathbf{x}', t') = \eta(\mathbf{x}' + \lambda \epsilon t', t')$ . Let us examine the correlations in the noise  $\eta'$ :

$$\begin{aligned} \langle \eta'(\mathbf{x}_1, t_1) \eta'(\mathbf{x}_2, t_2) \rangle &= \langle \eta(\mathbf{x}_1 + \lambda \epsilon t_1, t_1) \eta(\mathbf{x}_2 + \lambda \epsilon t_2, t_2) \rangle \\ &= F(\mathbf{x}_1 - \mathbf{x}_2 + \lambda \epsilon (t_1 - t_2), t_1 - t_2). \end{aligned} \quad (\text{B4})$$

Here  $F$  measures the noise correlations in the original equation. In the absence of temporal correlations  $F(\mathbf{x}, t) = \delta(t)F(\mathbf{x})$  and from Eq. (B4), we observe that the correlations for the new noise  $\eta'$  are identical to that in the original equation; i.e.,

$$F'(\mathbf{x}, t) = F(\mathbf{x} + \lambda \epsilon t, t) = \delta(t)F(\mathbf{x} + \lambda \epsilon t) = \delta(t)F(\mathbf{x}). \quad (\text{B5})$$

This invariance is no longer true if  $F(\mathbf{x}, t)$  is not proportional to  $\delta(t)$ . Therefore the stochastic equations is invariant under Galilean transformations, only if the noise has no temporal correlations.

Note that the parameter  $\lambda$  appears both as the coefficient of the nonlinearity in Eq. (1.1) and as an inherent factor relating to  $\mathbf{x}$  and  $t$  reparametrizations in Eq. (B2). Hence any renormalization of the Burgers equation that preserves Galilean invariance must leave the coefficient  $\lambda$  unchanged. This is even more transparent in the original Eq.(1.1). Here the nonlinearity on the left-hand side (with  $\lambda=1$ ) originates from the *total derivative*  $D\mathbf{v}/Dt$ . After any rescaling, we still expect  $D\mathbf{v}/Dt$  to appear as a consequence of Newton's law. Hence to all orders in perturbation theory we expect  $\tilde{\lambda}=\lambda$ . Due to absence of corrections, Eq. (2.21c) is exact, leading to the exponent identity

$$\chi + z = 2. \quad (\text{B6})$$

Due to this identity there is only one scaling exponent if Galilean invariance is not broken by noise correlations. As shown in the following appendixes, in the presence of temporal correlations  $d\lambda/dl \neq 0$ . It is interesting that Eq. (B6) also emerges as a consequence of assuming a continuum elastic description for directed polymers in random media.<sup>9,5</sup> Krug<sup>42</sup> obtained this identity using a mode-coupling approximation on the interface growth equation. Also MRSB (Ref. 34) give this result by postulating a scale invariance for  $\lambda$ .

### APPENDIX C: PROPAGATOR RENORMALIZATION

We start from the symmetrized version of Eq. (2.11),

$$\begin{aligned} G(\mathbf{k}, \omega) = & G_0(\mathbf{k}, \omega) + 4 \left[ -\frac{\lambda}{2} \right]^2 G_0^2(\mathbf{k}, \omega) \\ & \times \int^\wedge d^{d'} q \frac{1}{(2\pi)^{d'}} \int_{-\infty}^{\infty} \frac{d\Omega}{2\pi} \left[ \left[ \mathbf{q} + \frac{\mathbf{k}}{2} \right] \cdot \left[ \mathbf{q} - \frac{\mathbf{k}}{2} \right] \right] \left[ \mathbf{k} \cdot \left[ \mathbf{q} + \frac{\mathbf{k}}{2} \right] \right] \\ & \times G_0 \left[ \left[ \mathbf{q} - \frac{\mathbf{k}}{2} \right], \frac{\omega}{2} - \Omega \right] \left[ G_0 \left[ \left[ \mathbf{q} + \frac{\mathbf{k}}{2} \right], \frac{\omega}{2} + \Omega \right] \right]^2 2D \left[ \left[ \mathbf{q} + \frac{\mathbf{k}}{2} \right], \frac{\omega}{2} + \Omega \right], \end{aligned}$$

where  $G_0(\mathbf{k}, \omega) = (\nu k^2 - i\omega)^{-1}$  is the bare propagator. The  $q$  integral is calculated in spherical coordinates:

$$\begin{aligned} G(\mathbf{k}, \omega) = & G_0(\mathbf{k}, \omega) + 4 \left[ -\frac{\lambda}{2} \right]^2 G_0^2(\mathbf{k}, \omega) \frac{S_{d'-1}}{(2\pi)^{d'}} \int_0^\wedge dq q^{d'-1} \int_0^\pi d\theta \sin^{d'-2}\theta \int_{-\infty}^{\infty} d\Omega \frac{1}{2\pi} \\ & \times \frac{\left[ q^2 - \frac{k^2}{4} \right] \left[ kq \cos\theta + \frac{k^2}{2} \right] 2D \left[ \left[ q^2 + kq \cos\theta + \frac{k^2}{4} \right]^{1/2}, \frac{\omega}{2} + \Omega \right]}{\left[ \nu \left[ q^2 - kq \cos\theta + \frac{k^2}{4} \right] - i \left[ \frac{\omega}{2} - \Omega \right] \right] \left[ \nu^2 \left[ q^2 + kq \cos\theta + \frac{k^2}{4} \right]^2 + \left[ \frac{\omega}{2} + \Omega \right]^2 \right]}, \end{aligned}$$

where  $\mathbf{k} \cdot \mathbf{q} \equiv kq \cos\theta$  and  $S_{d'}$  is the surface area of a  $d'$ -dimensional sphere. We look at  $G(\mathbf{k}, \omega)$  only to leading orders in  $k$  and  $\omega$ , which completely determines the behaviors of the system in the hydrodynamic regime of interest. The  $\omega \rightarrow 0$  limit can be taken right away. After changes of variables  $x \equiv k/q$  and  $z \equiv \Omega/\nu q^2$  to make the integration variables dimensionless, the propagator becomes

$$\begin{aligned} G(k, 0) = & G_0(k, 0) + G_0^2(k, 0) \int_0^\wedge dq q^{d'-1} \left[ \frac{\lambda^2}{\nu^2} \frac{S_{d'-1}}{(2\pi)^{d'}} \int_{-\infty}^{\infty} dz \frac{1}{\pi} \int_0^\pi d\theta \sin^{d'-2}\theta \right. \\ & \times \left. \frac{\left[ 1 - \frac{x^2}{4} \right] \left[ x \cos\theta + \frac{x^2}{2} \right] D \left[ q \left[ 1 + x \cos\theta + \frac{x^2}{4} \right]^{1/2}, \nu q^2 z \right]}{\left[ \left[ 1 - x \cos\theta + \frac{x^2}{4} \right] + iz \right] \left[ \left[ 1 + x \cos\theta + \frac{x^2}{4} \right]^2 + z^2 \right]} \right]. \end{aligned}$$

The leading order  $k$  dependence in the integrand is  $x^2$  and  $x^2 \cos^2 \theta$ , as the  $x \cos \theta$  term vanishes by symmetry upon angular integration.

Define the expression in  $\{ \dots \}$  above to be  $I(x, q)$ . Then to leading order in  $x$ ,

$$\begin{aligned}
 I(x, q) &= \frac{\lambda^2}{v^2} \frac{S_{d'-1}}{(2\pi)^{d'}} \int_{-\infty}^{\infty} dz \frac{1}{\pi} \int_0^{\pi} d\theta \sin^{d'-2} \theta \frac{\left[ x \cos \theta + \frac{x^2}{2} \right] \left[ D(q, vq^2 z) + \frac{x}{2} \cos \theta (\partial_q D) \right]}{(1 - x \cos \theta + iz)(1 + 2x \cos \theta + z^2)} \\
 &= \frac{\lambda^2}{v^2} \frac{S_{d'-1}}{(2\pi)^{d'}} \int_{-\infty}^{\infty} dz \frac{1}{\pi} \frac{1}{(1 + iz)(1 + z^2)} \int_0^{\pi} d\theta \sin^{d'-2} \theta \left[ 1 + \frac{x \cos \theta}{1 + iz} \right] \left[ 1 - \frac{2x \cos \theta}{1 + z^2} \right] \\
 &\quad \times \left[ x \cos \theta + \frac{x^2}{2} \right] \left[ D(q, vq^2 z) + \frac{x}{2} \cos \theta (\partial_q D) \right] \\
 &= \frac{\lambda^2}{v^2} \frac{S_{d'-1}}{(2\pi)^{d'}} \int_{-\infty}^{\infty} dz \frac{1}{\pi} \frac{1}{(1 + iz)(1 + z^2)} \\
 &\quad \times \int_0^{\pi} d\theta \sin^{d'-2} \theta \left[ x^2 \left[ \frac{1}{2} D(q, vq^2 z) \right] + x^2 \cos^2 \theta \left[ \frac{D(q, vq^2 z)}{1 + iz} - \frac{2D(q, vq^2 z)}{1 + z^2} + \frac{1}{2} \partial_q D(q, vq^2 z) \right] \right].
 \end{aligned}$$

The angular integrals are now easily evaluated by noting that

$$\frac{S_{d'-1}}{(2\pi)^{d'}} \int_0^{\pi} d\theta \sin^{d'-2} \theta = \frac{S_{d'}}{(2\pi)^{d'}} \equiv K_{d'}, \quad \int_0^{\pi} d\theta \sin^{d'-2} \theta \cos^2 \theta = \frac{1}{d'} \int_0^{\pi} d\theta \sin^{d'-2} \theta$$

and

$$\int_0^{\pi} d\theta \sin^{d'-2} \theta \cos^2 \theta = \frac{1}{d'} \int_0^{\pi} d\theta \sin^{d'-2} \theta$$

by symmetry. So

$$\begin{aligned}
 I(x, q) &= x^2 K_{d'} \frac{\lambda^2}{v^2} \int_{-\infty}^{\infty} dz \frac{1}{\pi} \left[ D(q, vq^2 z) \left[ \frac{1}{2} \frac{1}{(1 + iz)(1 + z^2)} - \frac{1}{d'} \frac{1}{(1 + z^2)^2} \right] \right. \\
 &\quad \left. + \frac{1}{(1 + iz)(1 + z^2)} \frac{1}{2d'} \partial_q D(q, vq^2 z) \right].
 \end{aligned}$$

Since  $D$  is even in  $z$ , the two  $z$  integrals it multiplies are identical. If we define

$$\tilde{D}_1(q) = \frac{2}{\pi} \int_{-\infty}^{\infty} dz \frac{D(q, vq^2 z)}{(1 + z^2)^2}, \tag{C1}$$

then

$$I(x, q) = x^2 K_{d'} \frac{\lambda^2}{v^2} \left[ \frac{d'-2}{4d'} \tilde{D}_1(q) + \frac{1}{4d'} \partial_q \tilde{D}_1(q) \right] = x^2 K_{d'} \frac{\lambda^2 \tilde{D}_1(q)}{v^2} \frac{d'-2 + \tilde{f}_1(q)}{4d'},$$

where

$$\tilde{f}_1(q) \equiv \frac{2}{\pi} \int_{-\infty}^{\infty} dz \frac{1}{(1 + z^2)^2} \frac{\partial \ln D(k, \omega)}{\partial \ln k} \Bigg|_{\substack{k=q \\ \omega=vq^2 z}}.$$

The propagator becomes

$$G(k, 0) = G_0(k, 0) + G_0^2(k, 0) K_{d'} \frac{\lambda^2}{v^2} k^2 \int_0^{\Lambda} dq q^{d'-1} q^{-2} \tilde{D}_1(q) \frac{d'-2 + \tilde{f}_1(q)}{4d'}. \tag{C2}$$

In the special case of  $D(k, \omega) = D(k) = Dk^{-2\rho}$ , the integral in (C1) can be easily evaluated,

$$\tilde{D}_1(q) = D(q), \quad \tilde{f}_1(q) = -2\rho. \tag{C3}$$

The  $q$  integral in (C2) has an infrared divergence for  $d < d_c$  as discussed in Sec. II A. The renormalization procedure outlined there is used to tame the singularity. Integrating over the outer shell momenta  $\Lambda(1-\delta l) < q < \Lambda$ , where  $\delta l$  is infinitesimal, and setting  $\Lambda$  to unity,

$$\begin{aligned} G^<(k,0) &= G_0(k,0) + G_0^2(k,0) K_{d'} \frac{\lambda^2 \tilde{D}_1(1)}{v^2} k^2 \delta l \frac{d'-2+\tilde{f}_1(1)}{4d'} \\ &= G_0(k,0) \left[ 1 + \delta l K_{d'} \frac{\lambda^2 \tilde{D}_1(1)}{v^3} \frac{d'-2+\tilde{f}_1(1)}{4d'} \right], \end{aligned}$$

or

$$v^< = v \left[ 1 - \delta l K_{d'} \frac{\lambda^2 \tilde{D}_1(1)}{v^3} \frac{d'-2+\tilde{f}_1(1)}{4d'} \right].$$

Now the variables are rescaled:  $k \rightarrow (1-\delta l)k$ ,  $\omega \rightarrow (1-z\delta l)\omega$ ,  $h \rightarrow (1-\chi\delta l)h$ . The renormalized effective surface tension  $\tilde{v}$  is related to  $v^<$  by simple dimension counting similar to Eq. (2.6),

$$\tilde{v} = v + \frac{dv}{dl} \delta l = v^< [1 + \delta l(z-2)].$$

Hence the differential recursion relation for  $v$  is

$$\frac{dv}{dl} = v \left[ z-2 - K_{d'} \frac{\lambda^2 \tilde{D}_1(1)}{v^3} \frac{d'-2+\tilde{f}_1(1)}{4d'} \right]. \quad (\text{C4})$$

#### APPENDIX D: SPECTRAL-DENSITY FUNCTION RENORMALIZATION

We first compute the leading-order correction due to the elimination of high momenta modes. The relevant diagram is shown in Fig. 2(b); it has a multiplicity of 2. The details of the calculation will not be repeated here as they are similar to Appendix C. We have

$$\begin{aligned} 2D^<(k,\omega) &= 2D(k,\omega) + 2 \left[ -\frac{\lambda}{2} \right]^2 \int^> d^{d'} q \frac{1}{(2\pi)^{d'}} \int_{-\infty}^{\infty} d\Omega \frac{1}{2\pi} \left[ \left[ \mathbf{q} + \frac{\mathbf{k}}{2} \right] \cdot \left[ \mathbf{q} - \frac{\mathbf{k}}{2} \right] \right]^2 \\ &\quad \times \left| G_0 \left[ \left[ \mathbf{q} + \frac{\mathbf{k}}{2} \right], \frac{\omega}{2} + \Omega \right] \right|^2 \left| G_0 \left[ \left[ \mathbf{q} - \frac{\mathbf{k}}{2} \right], \frac{\omega}{2} - \Omega \right] \right|^2 \\ &\quad \times 2D \left[ \left[ \mathbf{q} + \frac{\mathbf{k}}{2} \right], \frac{\omega}{2} + \Omega \right] 2D \left[ \left[ \mathbf{q} - \frac{\mathbf{k}}{2} \right], \frac{\omega}{2} - \Omega \right] \\ &= 2D(k,\omega) + \delta l 2 \frac{\lambda^2}{v^3} \frac{S_{d'-1}}{(2\pi)^{d'}} \int_{-\infty}^{\infty} dz \frac{1}{2\pi} \int_0^\pi d\theta \sin^{d'-2}\theta \frac{D \left[ 1, vz + \frac{\omega}{2} \right] D \left[ 1, vz - \frac{\omega}{2} \right]}{(1+z^2)^2} \quad \text{for } k, \omega \rightarrow 0 \\ &= 2D(k,\omega) + 2\delta l K_{d'} \frac{\lambda^2}{4v^3} \tilde{D}_2^<(\omega) \quad \text{for } k \in [0, 1-\delta l], \end{aligned}$$

where

$$\tilde{D}_2^<(\omega) \equiv \frac{2}{\pi} \int_{-\infty}^{\infty} dz \frac{D \left[ 1, vz + \frac{\omega}{2} \right] D \left[ 1, vz - \frac{\omega}{2} \right]}{(1+z^2)^2} = \frac{2}{\pi} \int_{-\infty}^{\infty} dz \frac{D^2(1, vz)}{(1+z^2)^2}, \quad \omega \rightarrow 0. \quad (\text{D1})$$

Again, for the special case of  $D(k,\omega) = D(k)$ , (D1) reduces to  $\tilde{D}_2^< = D^2(1)$ , leading to Eq. (2.20). Now perform rescaling to get back to the original Brillouin zone,

$$\begin{aligned} \tilde{D}(k,\omega) &= D^<((1-\delta l)k, (1-z\delta l)\omega) [1 + \delta l(z-2\chi-d')] \\ &= D(k,\omega) + \delta l \left[ (z-2\chi-d')D(k,\omega) - k \frac{\partial D}{\partial k} - z\omega \frac{\partial D}{\partial \omega} + K_{d'} \frac{\lambda^2}{4v^3} \tilde{D}_2^<(\omega) \right]. \end{aligned}$$

We obtain the following functional integral-differential recursion relation for the spectral density function:

$$\frac{d}{dl} D(k, \omega) = D(k, \omega) \left[ z \left[ 1 - \frac{\partial \ln D(k, \omega)}{\partial \ln \omega} \right] - 2\chi - d' - \frac{\partial \ln D(k, \omega)}{\partial \ln k} \right] + K_{d'} \frac{\lambda^2}{4\nu^3} \tilde{D}_2(\omega). \quad (\text{D2})$$

### APPENDIX E: VERTEX RENORMALIZATION

We calculate the three-point vertex function  $\Gamma$  at the symmetrized point. There are three distinct one-loop diagrams contributing to the correction to the vertex as shown in Fig. 2(c). These diagrams all have multiplicity 4. Let  $\hat{k}_i \equiv (\mathbf{k}_i, \omega_i)$ ,  $\hat{q} \equiv (\mathbf{q}, \Omega)$ ,  $\mathbf{k}_i \cdot \mathbf{q} = k_i q \cos \theta_i$ ; we proceed with elimination of high momenta for the first diagram,

$$\begin{aligned} \Gamma_a^{\leq} \left[ \hat{k}_1, \frac{\hat{k}_1}{2} + \hat{k}_2, \frac{\hat{k}_1}{2} - \hat{k}_2 \right] &= \Gamma_0 \left[ \hat{k}_1, \frac{\hat{k}_1}{2} + \hat{k}_2, \frac{\hat{k}_1}{2} - \hat{k}_2 \right] \\ &\times \left\{ 1 + \frac{4(-\lambda/2)^2}{(\mathbf{k}_1/2 + \mathbf{k}_2) \cdot (\mathbf{k}_1/2 - \mathbf{k}_2)} \right. \\ &\times \int \int^> d^{d'} q d\Omega \frac{1}{(2\pi)^{d'}} \left[ \left[ \mathbf{q} + \frac{\mathbf{k}_1}{2} \right] \cdot \left[ \mathbf{q} - \frac{\mathbf{k}_1}{2} \right] \right] \\ &\times \left[ \left[ \frac{\mathbf{k}_1}{2} - \mathbf{k}_2 \right] \cdot (\mathbf{q} - \mathbf{k}_2) \right] \left[ \left[ \frac{\mathbf{k}_1}{2} + \mathbf{k}_2 \right] \cdot (\mathbf{q} - \mathbf{k}_2) \right] \\ &\times G_0 \left[ \frac{\hat{k}_1}{2} + \hat{q} \right] G_0 \left[ \frac{\hat{k}_1}{2} - \hat{q} \right] \left| G_0(\hat{q} - \hat{k}_2) \right|^2 2D(\hat{q} - \hat{k}_2) \left. \right\} \\ &= 1 + \delta l \frac{\lambda^2}{\nu^3} \frac{S_{d'-1}}{(2\pi)^{d'}} \int_{-\infty}^{\infty} dz \frac{1}{\pi} \frac{D(1, \nu z)}{(1+z^2)^2} \int d\theta_1 \sin^{d'-2} \theta_1 \frac{(k_1/2)^2 \cos^2 \theta_1 - k_2^2 \cos^2 \theta_2}{(k_1/2)^2 - k_2^2}, \end{aligned}$$

where  $\Gamma_0(\hat{k}_a + \hat{k}_b, \hat{k}_a, \hat{k}_b) = -(\lambda/2) \mathbf{k}_a \cdot \mathbf{k}_b G_0(\hat{k}_a) G_0(\hat{k}_b)$  is the bare vertex function.

The two angular integrals are identical by a shift of integration variable, so

$$\Gamma_a^{\leq} = \Gamma_0 \left[ 1 + \delta l K_{d'} \frac{\lambda^2}{\nu^3} \frac{1}{d'} \int_{-\infty}^{\infty} dz \frac{1}{\pi} \frac{D(1, \nu z)}{(1+z^2)^2} \right] = \Gamma_0 \left[ 1 + \delta l K_{d'} \frac{\lambda^2 \tilde{D}_1(1)}{\nu^3} \frac{1}{d'} \right],$$

where  $\tilde{D}_1(1)$  is as given in (C1).

The remaining two diagrams are calculated similarly. They are equal in the  $k_1, k_2 \rightarrow 0$  limit,

$$\begin{aligned} \Gamma_b^{\leq} &= \Gamma_0 \left\{ 1 + \frac{4(-\lambda/2)^2}{(\mathbf{k}_1/2 + \mathbf{k}_2) \cdot (\mathbf{k}_1/2 - \mathbf{k}_2)} \int \int^> d^{d'} q d\Omega \frac{1}{(2\pi)^{d'}} \left[ \left[ \mathbf{q} + \frac{\mathbf{k}_1}{2} \right] \cdot \left[ \mathbf{q} - \frac{\mathbf{k}_1}{2} \right] \right] \right. \\ &\times \left[ - \left[ \frac{\mathbf{k}_1}{2} - \mathbf{k}_2 \right] \cdot (\mathbf{q} - \mathbf{k}_2) \right] \left[ \left[ \frac{\mathbf{k}_1}{2} + \mathbf{k}_2 \right] \cdot (\mathbf{q} - \mathbf{k}_2) \right] \\ &\times G_0 \left[ \frac{\hat{k}_1}{2} + \hat{q} \right] \left| G_0 \left[ \frac{\hat{k}_1}{2} - \hat{q} \right] \right|^2 G_0(\hat{q} - \hat{k}_2) 2D \left[ \frac{\hat{k}_1}{2} - \hat{q} \right] \left. \right\} \\ &= \Gamma_0 \left[ 1 - \delta l \frac{\lambda^2}{\nu^3} \frac{S_{d'-1}}{(2\pi)^{d'}} \int_{-\infty}^{\infty} dz \frac{1}{\pi} \frac{D(1, \nu z)}{(1+z^2)(1-iz)^2} \int d\theta \sin^{d'-2} \theta_1 \frac{(k_1/2)^2 \cos^2 \theta_1 - k_2^2 \cos^2 \theta_2}{(k_1/2)^2 - k_2^2} \right] \\ &= \Gamma_0 \left[ 1 - \delta l K_{d'} \frac{\lambda^2}{\nu^3} \frac{1}{d'} \int_{-\infty}^{\infty} dz \frac{1}{\pi} \frac{D(1, \nu z)}{(1+z^2)(1-iz)^2} \right] = \Gamma_c^{\leq}(k_1, k_2 \rightarrow 0). \end{aligned}$$

Combining the results:

$$\Gamma^< = \Gamma_a^< + \Gamma_b^< + \Gamma_c^< = \Gamma_0 \left[ 1 - \delta l K_{d'} \frac{\lambda^2 \bar{D}_3}{\nu^3} \frac{1}{2d'} \right],$$

where

$$\bar{D}_3 \equiv \frac{2}{\pi} \int_{-\infty}^{\infty} dz D(1, \nu z) \frac{1-3z^2}{(1+z^2)^3}. \quad (\text{E1})$$

For spatial correlation only, i.e.,  $D(q, \nu z) = D(q)$ , the integral vanishes, and  $\Gamma^< = \Gamma_0$ . This result is attributed to Galilean invariance, as discussed in Appendix B. Finally, the parameters are rescaled as done previously, leading to the recursion relation

$$\frac{d\lambda}{dl} = \lambda \left[ \chi + z - 2 - \frac{\lambda^2 \bar{D}_3}{\nu^3} \frac{1}{2d'} \right]. \quad (\text{E2})$$

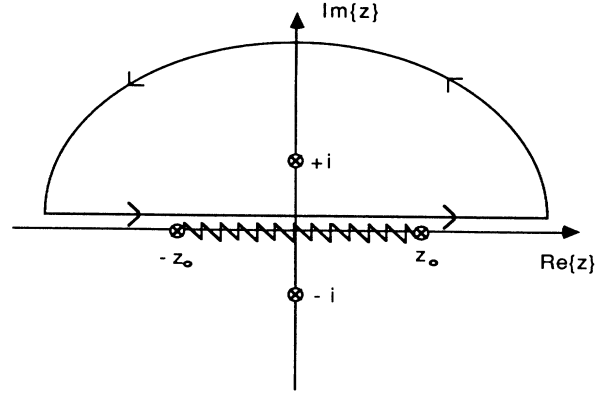


FIG. 10. Contours in complex  $z$  plane, used to perform the integrations in Appendix F.

#### APPENDIX F: FREQUENCY INTEGRAL FOR $\langle DD \rangle$ CONTRACTION

We want to evaluate the integral involved in contraction of the  $i$ th and  $j$ th term of the spectral density function  $D(\omega) = D_0 + \sum_n D_n \omega^{-2\theta_n}$ , where  $\theta_n = n\theta - (n-1)/2$ . The relevant integral to do is Eq. (D1). Here we compute one generic term,

$$\begin{aligned} I &= \frac{1}{2} \left[ \int_{-\infty}^{+\infty} dz \frac{\left| z + \frac{\omega}{2\omega_0} \right|^{-2\theta_i} \left| z - \frac{\omega}{2\omega_0} \right|^{-2\theta_j}}{(1+z^2)^2} + \int_{-\infty}^{+\infty} dz \frac{\left| z + \frac{\omega}{2\omega_0} \right|^{-2\theta_i} \left| z - \frac{\omega}{2\omega_0} \right|^{-2\theta_j}}{(1+z^2)^2} \right] \\ &= \int_{\omega/2\omega_0}^{\infty} dz \frac{\left[ z + \frac{\omega}{2\omega_0} \right]^{-2\theta_i} \left[ z - \frac{\omega}{2\omega_0} \right]^{-2\theta_j}}{(1+z^2)^2} + \int_{\omega/2\omega_0}^{\infty} dz \frac{\left[ z + \frac{\omega}{2\omega_0} \right]^{-2\theta_j} \left[ z - \frac{\omega}{2\omega_0} \right]^{-2\theta_i}}{(1+z^2)^2} \\ &\quad + \int_{-\omega/2\omega_0}^{\omega/2\omega_0} dz \frac{\left[ \frac{\omega}{2\omega_0} + z \right]^{-2\theta_i} \left[ \frac{\omega}{2\omega_0} - z \right]^{-2\theta_j}}{(1+z^2)^2}. \end{aligned}$$

In the limit  $\omega \rightarrow 0$ , the last term above becomes

$$\begin{aligned} I_1 &\equiv \int_{-\omega/2\omega_0}^{\omega/2\omega_0} dz \frac{\left[ \frac{\omega}{2\omega_0} + z \right]^{-2\theta_i} \left[ \frac{\omega}{2\omega_0} - z \right]^{-2\theta_j}}{(1+z^2)^2} \\ &\approx \int_{-\omega/2\omega_0}^{\omega/2\omega_0} dz \left[ \frac{\omega}{2\omega_0} + z \right]^{-2\theta_i} \left[ \frac{\omega}{2\omega_0} - z \right]^{-2\theta_j} [1 + O(z^2)] \\ &= \left[ \frac{\omega}{\omega_0} \right]^{1-2\theta_i-2\theta_j} \int_0^1 d\xi \xi^{-2\theta_i} (1-\xi)^{-2\theta_j} + O \left[ \frac{\omega}{\omega_0} \right]^{3-2\theta_i-2\theta_j} \\ &= \left[ \frac{\omega}{\omega_0} \right]^{1-2\theta_i-2\theta_j} \frac{\Gamma(1-2\theta_i)\Gamma(1-2\theta_j)}{\Gamma(2-2\theta_i-2\theta_j)} + O \left[ \frac{\omega}{\omega_0} \right]^{3-2\theta_i-2\theta_j}. \end{aligned}$$

From definition of  $\theta_n$  above, we have  $n(1-2\theta) = 1-2\theta_n$ . Hence

$$I_1 = \left[ \frac{\omega}{\omega_0} \right]^{-2\theta_i+j} \frac{\Gamma(1-2\theta_i)\Gamma(1-2\theta_j)}{\Gamma(1-2\theta_{i+j})} + O \left[ \frac{\omega}{\omega_0} \right]^{2-2\theta_{i+j}}. \quad (\text{F1})$$

We now turn to the other two pieces of  $I$ . Consider the following integral taken along the contour as shown in Fig. 10:

$$\begin{aligned}
 I_2(i, j) &= \oint_C dz \frac{\left[ z + \frac{\omega}{2\omega_0} \right]^{-2\theta_i} \left[ z - \frac{\omega}{2\omega_0} \right]^{-2\theta_j}}{(1+z^2)^2} \\
 &= e^{-2\pi i(\theta_i + \theta_j)} \int_{\omega/2\omega_0}^{\infty} dx \frac{\left[ x - \frac{\omega}{2\omega_0} \right]^{-2\theta_i} \left[ x + \frac{\omega}{2\omega_0} \right]^{-2\theta_j}}{(1+x^2)^2} \\
 &\quad + \int_{\omega/2\omega_0}^{\infty} dx \frac{\left[ x + \frac{\omega}{2\omega_0} \right]^{-2\theta_i} \left[ x - \frac{\omega}{2\omega_0} \right]^{-2\theta_j}}{(1+x^2)^2} + e^{-2\pi i\theta_j} \int_{-\omega/2\omega_0}^{\omega/2\omega_0} dx \frac{\left[ \frac{\omega}{2\omega_0} + x \right]^{-2\theta_i} \left[ \frac{\omega}{2\omega_0} - x \right]^{-2\theta_j}}{(1+x^2)^2}.
 \end{aligned}$$

Symmetric combination of  $I_2$ 's leads to

$$\begin{aligned}
 I_2(i, j) + I_2(j, i) &= 2\pi i \sum \text{Res}(I_2) = (e^{-2\pi i\theta_i} + e^{-2\pi i\theta_j}) \int_{-\omega/2\omega_0}^{\omega/2\omega_0} dx \frac{\left[ \frac{\omega}{2\omega_0} + x \right]^{-2\theta_i} \left[ \frac{\omega}{2\omega_0} - x \right]^{-2\theta_j}}{(1+x^2)^2} \\
 &\quad + (1 + e^{-2\pi i(\theta_i + \theta_j)}) \left[ \int_{\omega/2\omega_0}^{\infty} dx \frac{\left[ x + \frac{\omega}{2\omega_0} \right]^{-2\theta_i} \left[ x - \frac{\omega}{2\omega_0} \right]^{-2\theta_j}}{(1+x^2)^2} \right. \\
 &\quad \left. + \int_{\omega/2\omega_0}^{\infty} dx \frac{\left[ x + \frac{\omega}{2\omega_0} \right]^{-2\theta_j} \left[ x - \frac{\omega}{2\omega_0} \right]^{-2\theta_i}}{(1+x^2)^2} \right] \\
 &= I(1 + e^{-2\pi i(\theta_i + \theta_j)}) + I_1(e^{-2\pi i\theta_i} + e^{-2\pi i\theta_j} - 1 - e^{-2\pi i(\theta_i + \theta_j)}).
 \end{aligned}$$

We can now solve for the desired integral,

$$I = \frac{2\pi i \sum \text{Res}(I_2)}{1 + e^{-2\pi i(\theta_i + \theta_j)}} + I_1 \frac{(1 - e^{-2\pi i\theta_i})(1 - e^{-2\pi i\theta_j})}{1 + e^{-2\pi i(\theta_i + \theta_j)}}.$$

The second term is

$$\begin{aligned}
 \frac{2 \sin(\pi\theta_i) 2 \sin(\pi\theta_j)}{2 \cos[\pi(\theta_i + \theta_j)]} &= 2 \frac{\Gamma(1 - 2\theta_i)\Gamma(1 - 2\theta_j)}{\Gamma(1 - 2\theta_i + \theta_j)} \frac{2 \sin(\pi\theta_i) 2 \sin(\pi\theta_j)}{2 \sin(\pi\theta_i + \theta_j)} \left[ \frac{\omega}{\omega_0} \right]^{-2\theta_i + \theta_j} \\
 &\quad + O \left[ \left[ \frac{\omega}{\omega_0} \right]^{2 - 2\theta_i + \theta_j} \right].
 \end{aligned}$$

In the first term,

$$\begin{aligned}
 2\pi i \sum \text{res}(I_2) &= 2\pi i \frac{d}{dz} \left[ \frac{\left[ z + \frac{\omega}{2\omega_0} \right]^{-2\theta_i} \left[ z - \frac{\omega}{2\omega_0} \right]^{-2\theta_j}}{(i+z)^2} + \frac{\left[ z + \frac{\omega}{2\omega_0} \right]^{-2\theta_j} \left[ z - \frac{\omega}{2\omega_0} \right]^{-2\theta_i}}{(i+z)^2} \right]_{z=e^{i\pi/2}} \\
 &= \pi e^{-\pi i(\theta_i + \theta_j)} \left[ (1 + 2\theta_i + 2\theta_j) + O \left[ \left[ \frac{\omega}{\omega_0} \right]^2 \right] \right].
 \end{aligned}$$

Therefore

$$\begin{aligned} \bar{D}^2(\omega) = \frac{2}{\pi} I = \frac{1+2\theta_i+2\theta_j}{\cos[\pi(\theta_i+\theta_j)]} + \frac{4}{\pi} \frac{\Gamma(1-2\theta_i)\Gamma(1-2\theta_j)}{\Gamma(1-2\theta_{i+j})} \frac{2\sin(\pi\theta_i)2\sin(\pi\theta_j)}{2\sin(\pi\theta_{i+j})} \left[ \frac{\omega}{\omega_0} \right]^{-2\theta_{i+j}} \\ + O \left[ \left[ \frac{\omega}{\omega_0} \right]^{2-2\theta_{i+j}} \right] + O \left[ \left[ \frac{\omega}{\omega_0} \right]^2 \right]. \end{aligned} \quad (F2)$$

In the limit  $\theta_{i+j} \rightarrow 0$ ,  $\theta_i + \theta_j \rightarrow \frac{1}{2}$ ,

$$\bar{D}^2(\omega) \rightarrow \frac{2}{-\pi\theta_{i+j}} + \frac{4}{\pi} \Gamma(1-2\theta_i)\Gamma(2\theta_i) \frac{\sin(\pi\theta_i)\cos(\pi\theta_i)}{\pi\theta_{i+j}} \left[ 1 - 2\theta_{i+j} \ln \frac{\omega}{\omega_0} \right] + O(\theta_{i+j}^0).$$

Using the identity  $\Gamma(z)\Gamma(1-z) = \pi/\sin(\pi z)$ , we obtain:

$$\bar{D}^2(\omega) = -\frac{4}{\pi} \ln \frac{\omega}{\omega_0} + \text{const for } \theta_{i+j} = 0. \quad (F3)$$

- 
- <sup>1</sup>S. K. Ma, *Modern Theory of Critical Phenomena* (Benjamin, Reading, 1976).
- <sup>2</sup>P. C. Hohenberg and B. I. Halperin, *Rev. Mod. Phys.* **49**, 435 (1977), and references therein.
- <sup>3</sup>J. M. Burgers, *The Nonlinear Diffusion Equation* (Reidel, Boston, 1974).
- <sup>4</sup>D. Forster, D. R. Nelson, and M. J. Stephen, *Phys. Rev. A* **16**, 732 (1977).
- <sup>5</sup>M. Kardar, G. Parisi, and Y.-C. Zhang, *Phys. Rev. Lett.* **56**, 889 (1986).
- <sup>6</sup>H. van Beijeren, R. Kutner, and H. Spohn, *Phys. Rev. Lett.* **54**, 2026 (1985).
- <sup>7</sup>S. Zalesky, *Physica D* (to be published); G. I. Sivashinski, *Acta Astronautica* **6**, 569 (1979), and references therein.
- <sup>8</sup>M. Kardar and Y.-C. Zhang, *Phys. Rev. Lett.* **58**, 2087 (1987).
- <sup>9</sup>D. A. Huse, C. L. Henley, and D. S. Fisher, *Phys. Rev. Lett.* **55**, 2924 (1985), and references therein.
- <sup>10</sup>V. Yakhot and S. A. Orszag, *Phys. Rev. Lett.* **57**, 1722 (1986); V. Yakhot and Z.-S. She, *Phys. Rev. Lett.* **60**, 1840 (1988); and references therein.
- <sup>11</sup>M. Kardar, *J. Appl. Phys.* **61**, 3601 (1987).
- <sup>12</sup>T. Natterman, *Europhys. Lett.* **4**, 1241 (1987).
- <sup>13</sup>D. E. Wolf and J. Kertesz, *Europhys. Lett.* **4**, 651 (1987).
- <sup>14</sup>*Ill Condensed Matter*, 1978 Les Houches Lecture Notes, edited by R. Balian, R. Maynard, and G. Toulouse (North Holland, Amsterdam, 1979).
- <sup>15</sup>J. Villain, *Phys. Rev. Lett.* **52**, 1543 (1984); G. Grinstein and J. F. Fernandez, *Phys. Rev. B* **29**, 6389 (1984); R. Bruinsma and G. Aeppli, *Phys. Rev. Lett.* **52**, 1547 (1984); and references therein.
- <sup>16</sup>J. F. Fernandez, G. Grinstein, Y. Imry, and S. Kirkpatrick, *Phys. Rev. Lett.* **51**, 203 (1983).
- <sup>17</sup>M. Kardar, *Nucl. Phys.* **B290**, 582 (1987).
- <sup>18</sup>D. A. Huse and C. L. Henley, *Phys. Rev. Lett.* **54**, 2708 (1985).
- <sup>19</sup>M. Kardar, *Phys. Rev. Lett.* **55**, 2923 (1985).
- <sup>20</sup>A. Bovier, J. Frohlich, and U. Glaus, *Phys. Rev. B* **34**, 6409 (1986).
- <sup>21</sup>Y.-C. Zhang, *J. Phys. A* **19**, 1941 (1986).
- <sup>22</sup>M. Kardar and Y.-C. Zhang, *Europhys. Lett.* (to be published).
- <sup>23</sup>B. Derrida and H. Spohn (unpublished).
- <sup>24</sup>H. E. Stanley, *On Growth and Form: Fractal and Non-Fractal Patterns in Physics* (Dordrecht, Netherlands, 1986).
- <sup>25</sup>H. Leamy, G. Gilmer and A. G. Dirks, in *Current Topics in Material Science*, edited by E. Kaldis (North-Holland, Amsterdam, 1980), Vol. 6.
- <sup>26</sup>S. F. Edwards and D. R. Wilkinson, *Proc. R. Soc. London, Ser. A* **381**, 17 (1982).
- <sup>27</sup>R. Bausch, V. Dohm, H. K. Janssen, and R. K. P. Zia, *Phys. Rev. Lett.* **47**, 1837 (1981).
- <sup>28</sup>R. Ramanlal and L. M. Sander, *Phys. Rev. Lett.* **54**, 1828 (1985).
- <sup>29</sup>J. Krug and H. Spohn, *Phys. Rev. A* **38**, 4271 (1988).
- <sup>30</sup>F. Family and T. Vicsek, *J. Phys. A* **18**, L75 (1985).
- <sup>31</sup>M. Plischke and Z. Racz, *Phys. Rev. A* **32**, 3825 (1985).
- <sup>32</sup>R. Jullien and R. Botet, *Phys. Rev. Lett.* **54**, 2055 (1985); *J. Phys. A* **18**, 2279 (1985).
- <sup>33</sup>J. G. Zabolitzky and D. Stauffer, *Phys. Rev. A* **34**, 1523 (1986); *Phys. Rev. Lett.* **57**, 1809 (1986).
- <sup>34</sup>P. Meakin, P. Ramanlal, L. M. Sander, and R. C. Ball, *Phys. Rev. A* **34**, 5091 (1986).
- <sup>35</sup>M. Plischke, Z. Racz, and D. Liu, *Phys. Rev. B* **35**, 3485 (1987). See also D. Liu and M. Plischke (unpublished).
- <sup>36</sup>D. Dhar, *Phase Transitions* **9**, 51 (1987).
- <sup>37</sup>R. Jullien and P. Meakin, *Europhys. Lett.* **4**, 1385 (1987).
- <sup>38</sup>D. E. Wolf and J. Kertesz, *J. Phys. A* **20**, L257 (1987), and references therein.
- <sup>39</sup>A. J. McKane and M. A. Moore, *Phys. Rev. Lett.* **60**, 527 (1988).
- <sup>40</sup>See, however, A. Bunde, H. J. Hermann, A. Margolina, and H. E. Stanley, *Phys. Rev. Lett.* **55**, 653 (1985).
- <sup>41</sup>U. Dekker and F. Haake, *Phys. Rev. A* **11**, 2043 (1975).
- <sup>42</sup>J. Krug, *Phys. Rev. A* **36**, 5465 (1987).